AN ABSTRACT OF THE THESIS OF

ROGER LEE BLAINE (Name) for the DOCTOR OF PHILOSOPHY (Degree)

in CHEMISTRY (Major) presented on January 21, 1969 (Date)

Title: OPTIMIZATION OF THE CONTINUOUS ANALYSIS PEARL-BENSON METHOD FOR LIGNOSULFONATES

Redacted for Privacy

Abstract approved _____
Dr. Harry Freund

A procedure is described for the optimization of a previously described continuous analysis adaptation of the Pearl-Benson or nitroso method for estimation of spent sulfite liquor (SSL) or lignosulfonates. The optimized procedure has a response time of 6.5 minutes. In order to monitor samples whose SSL concentration is between 0 and 10 ppm, a long path length, dual beam, flow through colorimeter was developed. The colorimeter has a range of 0.94 absorbance units for a 10 cm cuvette length, and has a readout which expresses the sample concentration directly in millivolts. Both the continuous analysis chemical manipulation system and the colorimeter are packaged as portable units.

An empirical equation is obtained for the response curve of continuous analyzers. This equation permits simulation of the continuous analyzer response in both a mathematical form and on an analog computer. Examination of the electrical analog leads to

information about the response of continuous analysis apparatus to a variety of input signals and provides an approach to figures of merit for comparison of continuous analysis systems. An electronic method is illustrated for predicting the steady state value of a continuous analysis apparatus long before that steady state condition is obtained.

Optimization of the Continuous Analysis Pearl-Benson Method for Lignosulfonates

by

Roger Lee Blaine

A THESIS

submitted to

Oregon State University

in partial fulfillment of
the requirements for the
degree of

Doctor of Philosophy

June 1969

APPROVED:

Redacted for Privacy

Professor of Chemistry
in charge of major

Redacted for Privacy

Chairman of the Department of Chemistry

Redacted for Privacy

Dean of Graduate School

Date thesis is presented January 21, 1969

Typed by Gwendolyn Hansen for Roger Lee Blaine

ACKNOWLEDGMENTS

The author wishes to thank Dr. Harry Freund, one of whose purposes in life is to be mentor and catalyst in the preparation of complete, professional chemists. He has served the author admirably in this regard during the last few years and his reflection will continue to do so in the future.

The work leading to this thesis would have progressed much more slowly were it not for the contributions of my colleagues in the analytical division. In particular, the bibliography does not do proper credit to the contribution of Dr. Gary Olson.

The author also wishes to thank Burr-Brown Research Corporation for use of the Model 600 Analog Simulator used in this investigation and Northwest Pulp and Paper Association, Donald Benson executive secretary, who supported this research.

TABLE OF CONTENTS

LIST OF FIGURES

LIST OF TABLES

OPTIMIZATION OF THE CONTINUOUS ANALYSIS PEARL-BENSON METHOD FOR LIGNOSULFONATES

INTRODUCTION

Continuous chemical analysis, as defined by Blaedel and Laessig (4), is a chemical analysis in which the measurement step is performed on a flowing stream of sample. Colorimetric continuous analysis, introduced by Skeggs (28) some twelve years ago and popularized in recent years by Technicon Instrument Corporation (Ardsley, N. Y.), has become a popular method for monitoring pollutants in natural waters (29, 30, 31, 32).

One pollutant appearing in the waters of the Pacific Northwest and elsewhere, is spent sulfite liquor (SSL), a pulp mill waste product. The standard method for estimation of SSL concentrations is the Pearl-Benson or nitroso color reaction (3). The lignosulfonates, upon which the reaction depends, represent only 60% of the 10% nonvolatile solids present in the SSL (13). Acetic acid and sodium nitrite, when added to a water sample containing lignosulfonates, react to give the nitrosolignin. If this solution is then made basic by the addition of ammonium hydroxide, the tautomeric ligninquinone oxime is formed. Measurement of the yellow color of the quinoidal solution at 430 mμ (15), when compared to a reference sample in which the reagents have been added in the reverse order, gives an estimation of the lignosulfonates present. The slightly yellow color

of the nitrite and lignosulfonates plus the possibility that the water samples may contain other "yellow substances" necessitates the dual beam approach. Since the reference sample is never made acidic and thus the nitroso reaction does not take place, the reference sample provides an estimation of this "background" color. Furthermore, the levels of tens of parts per million SSL and less commonly encountered in natural waters necessitates the use of long path length colorimeters for the determination.

The Pearl-Benson method has been adapted to a continuous analysis procedure by Olson (20). His apparatus, however, was limited, by the short pathlength (1.0 cm) of the Beckman DB spectrophotometer used as a detector, to determinations of samples an order of magnitude higher in concentration than expected in natural waters. Nonetheless, the basic principles of his procedure are sound, and with the development of a suitable colorimeter along with optimization and ruggedization of the apparatus, such a procedure could be of benefit to the laboratory technician performing Pearl-Benson Index determinations or possibly to continuous monitoring of natural water systems. One of the goals of this investigation is to produce such an apparatus.

To date most of the work done in continuous analysis has been in this area of adapting existing methods to available apparatus. Relatively little has been done to develop methods or apparatus

uniquely suited for the continuous analysis procedure. Exploitation of the unique character of continuous analysis has not been possible in the past because of a lack of theoretical understanding of the physical processes involved. If continuous analysis, which is now used almost exclusively as an integrating, monitoring technique, is ever to be used in nonintegrating or feedback control applications, a better understanding of the dynamics of the method is necessary. One path to such an understanding is the creation of an electrical analog for the continuous analysis system. The electrical analog could then be evaluated by the techniques commonly used in feedback control theory, rather than by evaluating a difficult fluid system. Similar uses of electrical analogs have already been found to aid in the understanding of gas chromatography (14), differential thermal analysis (35), and electroanalytical instrumentation (5, 24).

The optimization of the continuous analysis procedure presented herein, can be divided into two general areas. The first of these areas deals with the chemical optimization of a specific procedure, that of the Pearl-Benson method for lignosulfonates. The second area deals with the optimization of the generalized continuous analysis process through a study of models representing continuous analysis response.

CHEMICAL OPTIMIZATION OF THE PEARL-BENSON METHOD

In continuous analysis the various manipulative steps are performed by the particular arrangement of proportioning pump, flow tubing, etc. Often the safeguards built into a manual method, to minimize the influence of technician error, can be markedly relaxed in the continuous analysis adaptation because of the reproducibility of the apparatus. Herein lies one of the major advantages of continuous analysis. This reproducibility makes possible the optimization of the manual procedure. An optimized procedure is one in which the desired information is produced as quickly as possible consistent with other goals such as low cost and reliability.

In the case of the Pearl-Benson reaction, for example, Anderson (2) has shown that if the acetic acid concentration is increased to six times that of the standard method, the nitrosolignin reaction goes essentially to completion in about 25% of the time required in the standard method. Of course the increase in acid concentration would necessitate a corresponding increase in the base concentration required later in the procedure. The analytical information, however, would then be available in a much shorter period of time at no sacrifice in reliability.

The approach to optimization used here consists of starting with conditions which are known to produce the desired chemical reactions,

then varying the parameters one at a time in a logical order while observing the apparatus readout. The optimized condition, selected from a plot of the apparatus readout versus the varied parameter (to be consistant with other desirous results), is used during the optimization of the remaining parameters.

Apparatus

The continuous analysis apparatus and procedure used in this optimization investigation, shown in Figure 1, were similar to those of Olson (20) with the following modifications. A Harvard (Harvard Apparatus Co., Millis, Mass. 02054) Model 1512 positive displacement pump a was used for fluid proportioning. Ten of the twelve available channels were in service. The sample : acid : nitrite : base flow ratio of 1 : 0.1 : 0.1 : 0.1 ml per stroke was obtained by adjusting the proportion control on each channel until water pumped from vertical glass tubes of 41.7 and 13.6 mm id, respectively, fell at comparable rates. The positive displacement feature of the pump, removed the necessity for constant pressure heads on the reagent reservoirs. The first mixing coils b and wait loops c, in the parallel sample and reference streams, were 17.2 m in length of which 25% were the mixing coils. The second mixing coils d and connections to the debubblers e were 7.9 m in length of which 70% were the mixing coils. These fluid path lengths, constructed from 4 mm pyrex

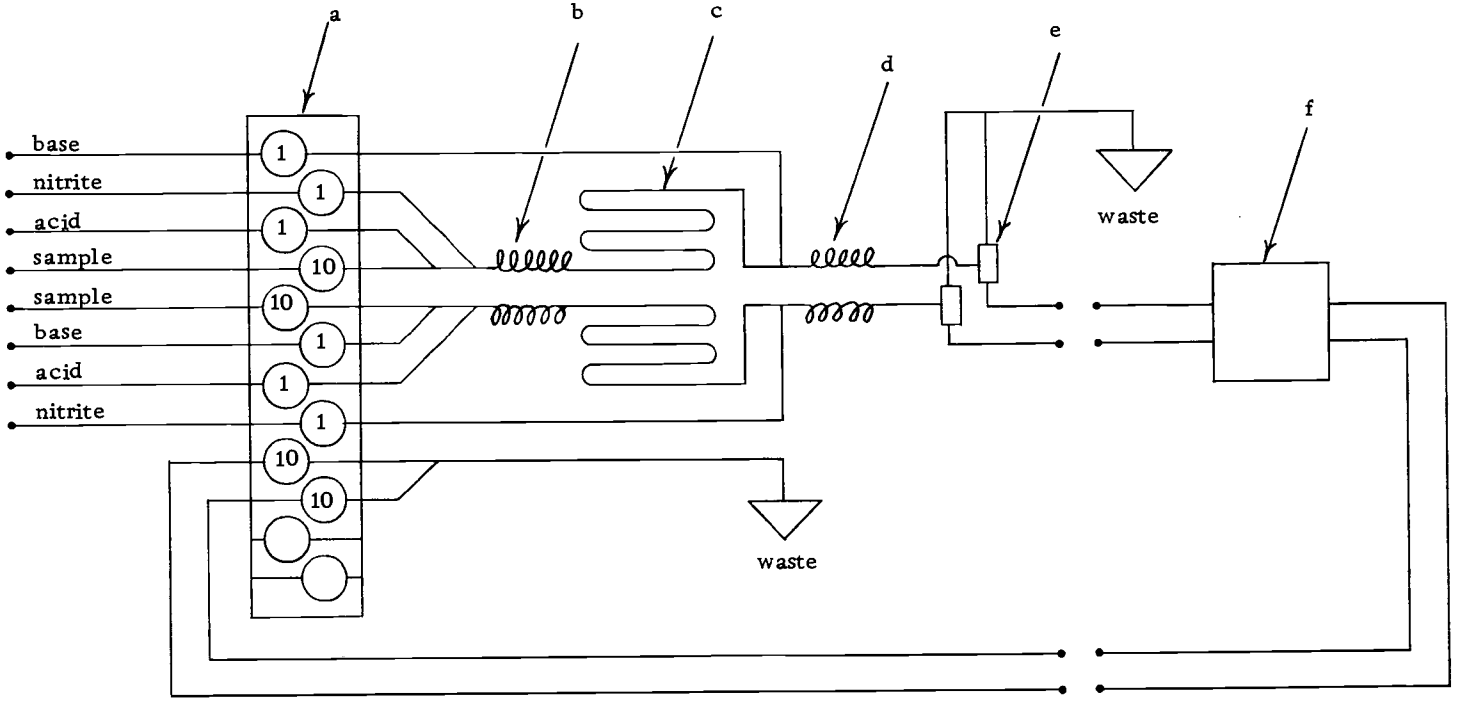

Figure 1. Schematic flow diagram used for optimization.

tubing, were chosen to give an estimated primary color time (the time required for the nitroso reaction to proceed essentially to completion) of five minutes at a pump speed of ten strokes per minute. The reference and sample streams are presented to a dual beam, flow through colorimeter f at the same time. A Beckman DB spectrophotometer with 1.0 cm cuvettes was used here.

Reagents

The sodium nitrite, acetic acid and ammonium hydroxide solutions used as reagents were prepared from reagent grade factory pack chemicals without further purification. The p-hydroxybenzoic acid solutions used in the study of interferences, were obtained by serial dilution from a 100 ppm stock solution. This stock solution was prepared by dissolving and diluting to 1.00 liter, 0.1003 grams of reagent grade p-hydroxybenzoic acid which had been dried at 110°C for 18 hours. The artificial seawater also used in the study of interferences was prepared by the method of Kester and co-workers (17). The solution was standardized by the Mohr titration and found to be 18.19 Cl‰.

Orzan A, a commercially available (Crown Zellerbach, Camas, Washington) form of ammonium lignosulfonates, containing 57% lignosulfonic acid, 15% reducing sugars, and 3% ammonia (9), was used as a typical example of the nonvolatile solids portion of SSL.

A 1.00 ppt stock solution of Orzan A was prepared by dissolving 1.000 grams of the vacuum dried powder and diluting to 1.00 liter with distilled water. The Orzan A standard solutions were obtained from this stock solution by serial dilution. The absorbance of synthetic SSL solutions (10% Orzan A) showed an absorptivity, for the optimized procedure, of 2.05×10^{-4} cm^{-1} ppm^{-1} SSL. When corrected for the difference in dilution brought about by the addition of reagents, this agrees with the absorptivity of 2.47×10^{-4} cm^{-1} ppm^{-1} SSL reported by Barnes and co-workers (3) for calcium based SSL.

Procedure

Optimization of the pump speed (and fluid flow rate) can take place once the approximate wait time for the development of the nitrosolignin, taken from reaction rate curves (2), has dictated the approximate volume of the fluid flow system. First approximation reagent concentrations of 1.7 F acetic acid, 0.29 F sodium nitrite, and 4.0 F ammonium hydroxide along with a 100 ppm Orzan A sample were supplied to the apparatus. The absorbance reading was observed as a function of pump speed. Figure 2 shows the dependence of the color intensity on the pump rate or the wait time. A pump rate of 20 strokes per minute (about 4 minutes wait time) was selected for the analysis consistent with the desire for maximum sensitivity

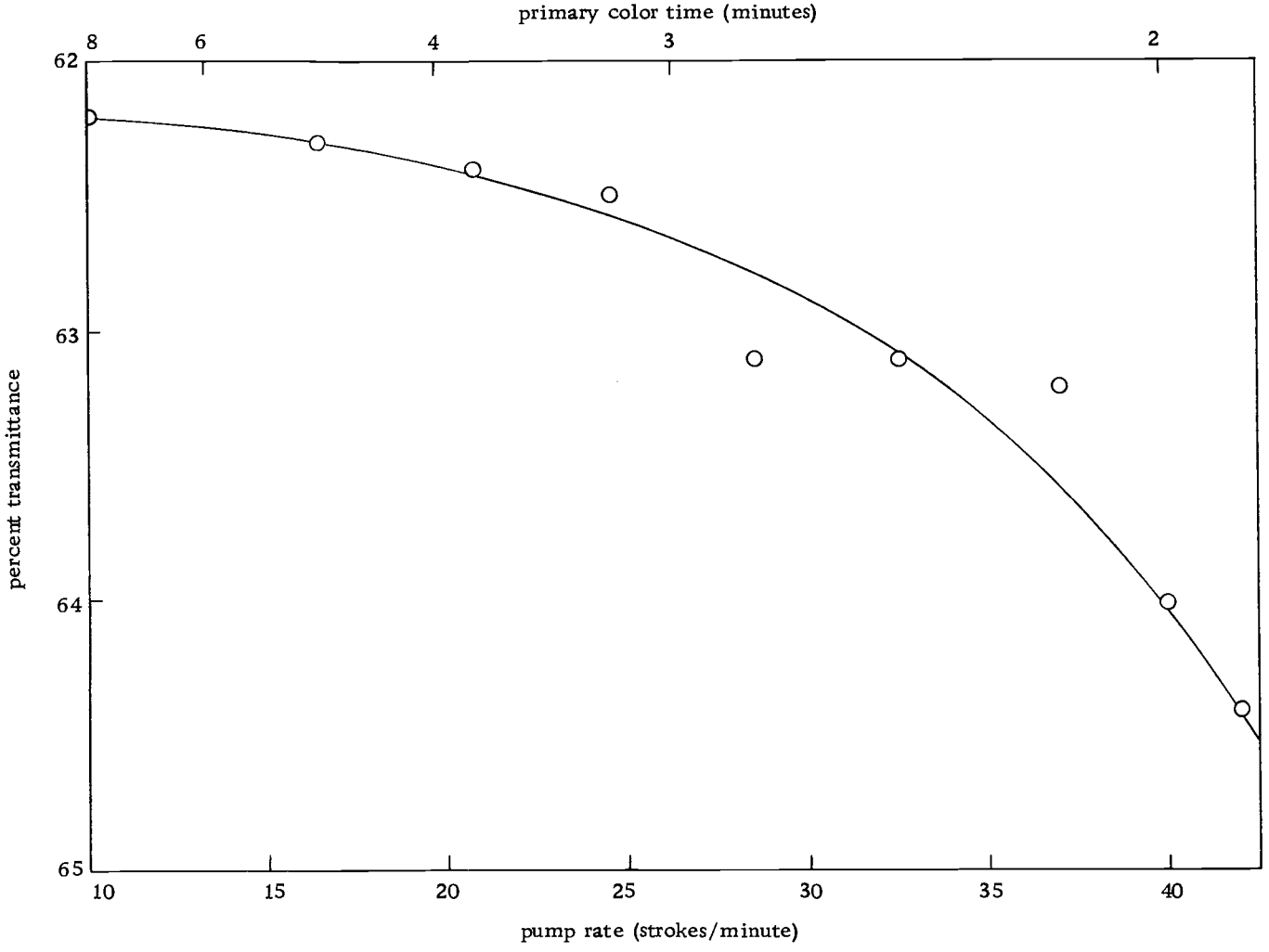

Figure 2. Dependence of color intensity on pump rate and primary color time (glass).

at minimum time.

Once the pump speed has been established, the next step in the optimization process is the selection of the appropriate reagent concentrations. The nitrite ion adduct should be the first object of attention. In order that this nitrite ion concentration not be reduced by relatively high concentrations of lignosulfonates, the sodium nitrite reagent concentration is established at a conveniently large value of 0.29 F.

Optimization of the acetic acid concentration is accomplished by observing the change in readout as a function of the acetic acid reagent concentration. Reagents and sample concentrations of 0.29 F sodium nitrite, 4.0 F ammonium hydroxide and 100 ppm Orzan A were supplied to the proportioning pump, operating at 23 strokes per minute. The dependence of the color development on the acetic acid concentration is shown in Figure 3. A concentration on the high absorbance plateau, close to the shoulder is required to minimize reagent cost. The conveniently prepared concentration of 1.7 F acetic acid was selected.

The optimization of the ammonium hydroxide concentration was carried out using the previously optimized parameters of 0.29 F sodium nitrite and 1.7 F acetic acid, together with 100 ppm Orzan A as a sample, pumped at 20 strokes per minute. The color intensity, as a function of ammonium hydroxide reagent concentration, (Figure 4)

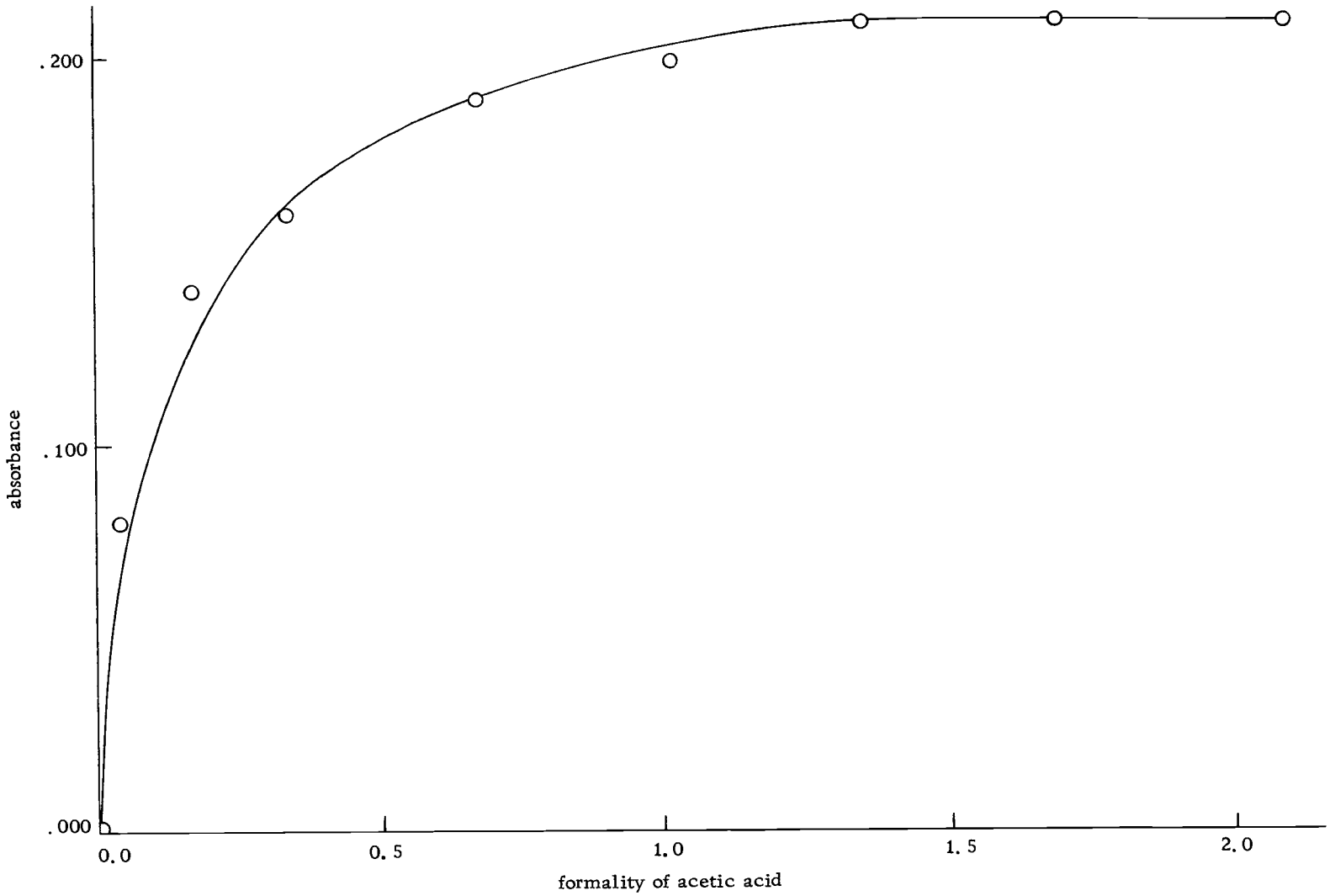

Figure 3. Dependence of color intensity on acid concentration.

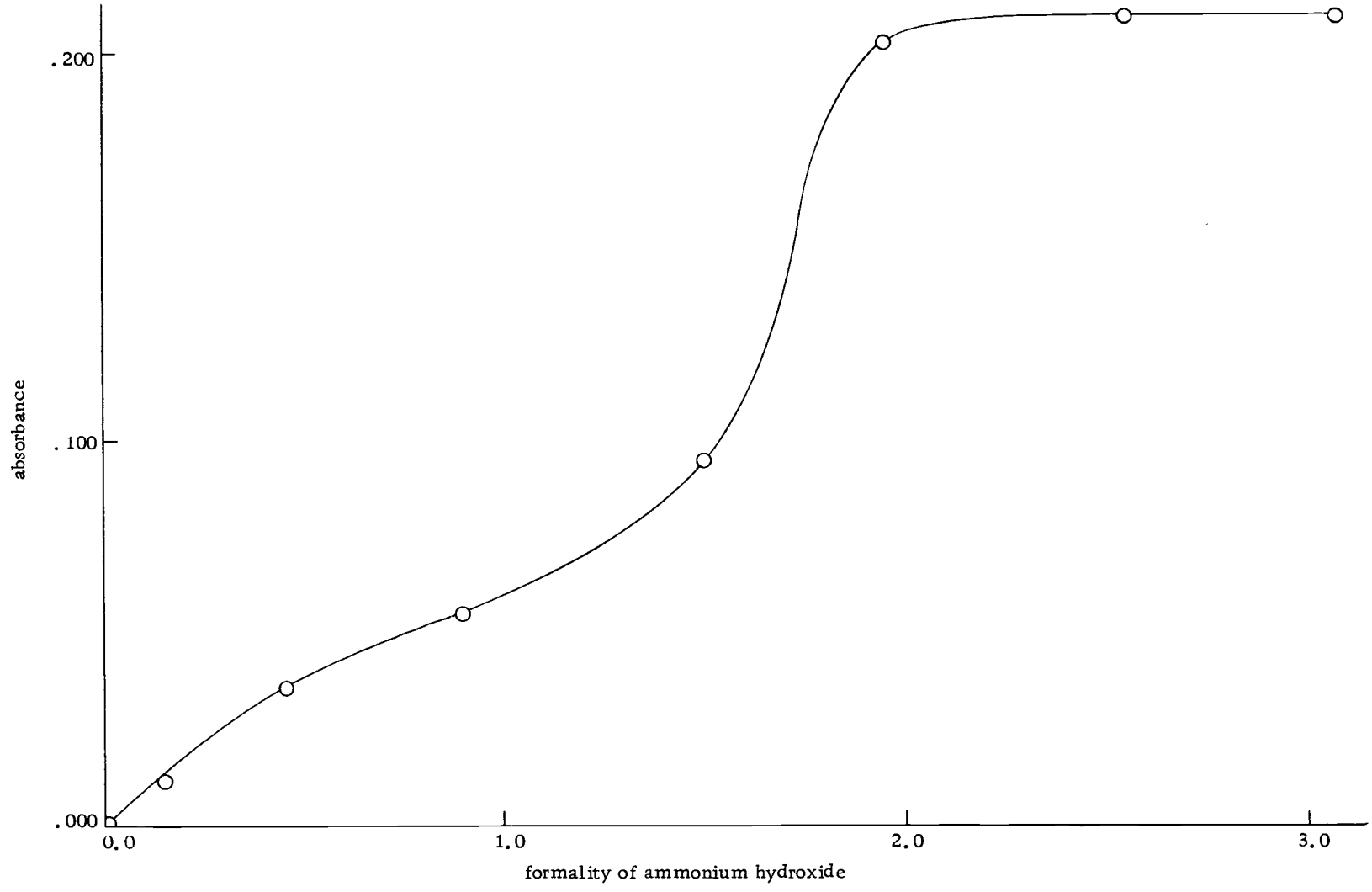

Figure 4. Dependence of color intensity on base concentration.

appears as a weak acid-base titration curve with the ligninquinone oxime serving an indicator. The 3.0 F ammonium hydroxide reagent concentration chosen as optimum provides a readout well onto the high absorbance plateau but produces a solution whose pH is less than ten. This is required because the magnesium in seawater, on which the Pearl-Benson determination is often run, precipitates as the hydroxide at about that pH (2).

The optimized parameters are collected in Table 1. The optimized reagent concentrations and the primary color wait time will be independent of the fluid flow path demensions. The pump speed, however, will depend upon the flow path volume of the particular apparatus used and upon the volume of sample and reagents pumped with each stroke.

Table 1. Collected Optimized Parameters

concentration of sodium nitrite	0.29 F
concentration of acetic acid	1.7 F
concentration of ammonium hydroxide	3.0 F
primary color wait time	4 minutes
pump speed	20 stk/min.

This particular procedure for optimization can easily be used to obtain information about the effects of suspected interferences.

For example, the intercept and slope of the analytical curve for the Pearl-Benson determination are different in seawater samples from those of fresh water (3). The difference in slope is probably due to the buffering effect of the seawater on the acidic and basic reagents. The intercept of 2 or 3 ppm SSL in seawater is attributable to interferences. Degens and co-workers (10) have observed total amounts of p-hydroxybenzoic, vanillic, and syringic acids in seawater of 1-3 μg/l. All three of these phenolic compounds are lignin degradation products and, if their absorptivity in the Pearl-Benson reaction were high enough, could serve as the offset in the analytical curve.

The effect of p-hydroxybenzoic acid as a possible interference was estimated by submitting various concentrations of the acid to the optimized continuous analysis apparatus for determination. The absorptivity of p-hydroxybenzoic acid was observed to be 1.8×10^{-3} cm^{-1} ppm^{-1}. Assuming that the absorptivity of vanillic and syringic acids will be of the same order of magnitude as that of the p-hydroxybenzoic acid then clearly the total levels of these acids in seawater is insufficient to cause the 2 or 3 ppm SSL background.

Artificial seawater, containing all of the chemical species found in natural seawater above the 1 ppm level, was also submitted to the optimized continuous analysis apparatus for determination. No detectable level of interference was observed.

PEARL-BENSON ANALYZER

With the optimized Pearl-Benson method at hand, attention can be given to packaging the continuous analysis apparatus so that the apparatus can be used where needed.

A modular approach was used in this packaging. Such an approach permits smaller size, better ventilation and increased portability of the equipment. It also permits the various pieces of equipment to be used in other systems if needed.

Of the various steps in an analysis (sampling, chemical manipulation, and readout) only the chemical manipulation and readout have progressed to the stage where actual packaging of equipment is possible.

Sample Preparation

Since the lignosulfonates are to be determined in a natural water matrix, some sort of sample preparation is necessary. The standard method (3) calls for settling for 12 to 24 hours and warming to room temperature. If after this settling period the sample is still turbid (defined as possessing an absorbance greater than 0.10 for a 10-cm cell at 600 mμ), the sample is filtered through a 0.80 μ cellulose ester filter. Clearly two steps are required for sample preparation: 1) clarification and 2) warming to some suitable

temperature.

Continuous centrifugation, such as performed by cyclone separators, has been suggested (21) as one means of clarifying natural waters for continuous analysis. To test centrifugation as a means of clarification, natural water samples taken from the Willamette River near Corvallis in November (after two weeks of intermittent rain) were centrifuged for one and a half minutes. Absorbance of the sample before and after the centrifugation was measured against distilled water using a Beckman DB spectrophotometer with 1.0 cm cuvettes. The absorbance was 0.170 at 428 mμ and 0.122 at 600 mμ before centrifugation and 0.045 and 0.016 afterward. This decrease in absorbance was comparable to that of settling overnight. According to the criterion of the standard method, the clarified solution is still too turbid for a determination. This is understandable since the background absorbance at 428 mμ would be nearly 20 times the expected absorbance of a 10 ppm SSL sample. Clearly additional clarification, such as filtration, would be required for the continuous (with time) monitoring of turbid natural water systems.

The second step in the sample preparation for continuous monitoring, that of warming the sample to some suitable temperature, would be relatively simple to accomplish. The sample, either before or after addition of the reagents, could be run through a thermostated bath.

Clearly the lack of ability for sample preparation in the following continuous analysis equipment limits its use to samples which have been previously clarified and warmed to room temperature by methods consistent with the standard Pearl-Benson method.

Chemical Manipulation

The ruggedized chemical manipulation system is basically that described earlier (in the optimization chapter) with the glass tubing replaced by less fragile teflon tubing.

A schematic diagram of the fluid flow system, with its connections to the colorimeter, is shown in Figure 5.

The proportioning pump a is a Harvard Apparatus Model 1512 pump. All twelve of the available channels are in service. The ratios of the flow for various channels were adjusted in the manner described in the optimization chapter.

The ruggedized mixing and time delay coils were constructed from AWG No. 10 teflon "spaghetti" tubing with tygon tubing (0.0625 inch wall, 0.25 inch o.d.) as connecting over-sleeving. The first mixing and time delay coils b consisted of winding 7.9 m of the teflon tubing onto cardboard cylinders (35 mm diameter, 35 cm length). The second mixing coils c were 1.9 m of the same teflon tubing wound over the first coil. Manifolds for insertion of reagents into the sample stream were 0.125 inch polypropylene "T" and "Y"

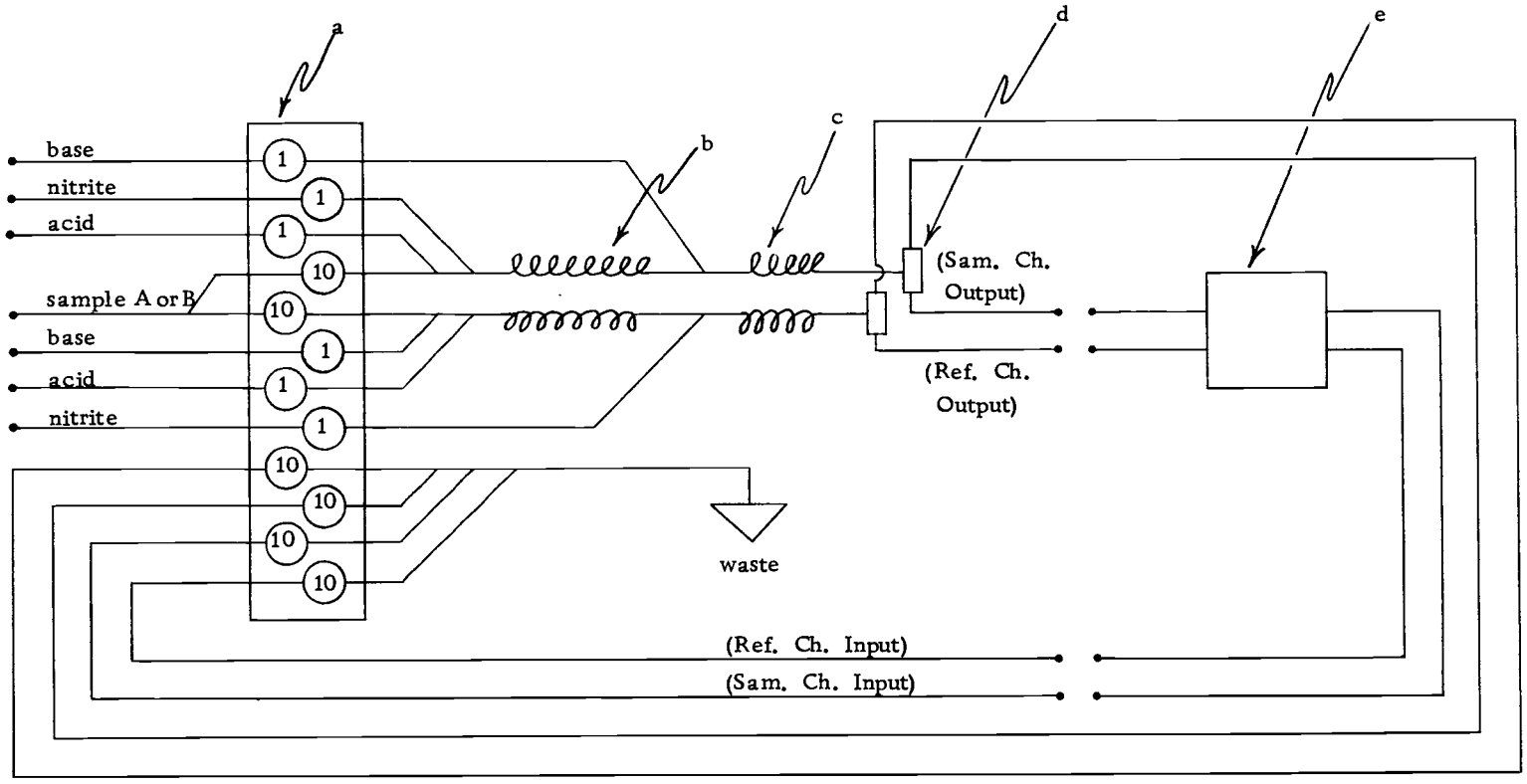

Figure 5. Schematic flow diagram of analyzer.

connectors (Cole-Parmer, Chicago, Illinois 60626). These mixing and time delay coils were mounted horizontally (Figure 6).

Two debubblers d remove any air bubbles in the fluid flow system before they reach the colorimeter e. An illustration of one of the debubblers is shown in Figure 7. Two side arms and one coaxial port (a, b, and c, respectively, in Figure 7), constructed from 4 mm pyrex tubing, extend from a 9 mm body d. The sample is injected into the device through the lower side arm b and is withdrawn through the coaxial port c. Any air bubbles in the sample rise to the top of the solution and are drawn off, along with any excess sample, through the upper side arm a. The vent hole e keeps this point in the fluid flow system open to the atmosphere. The two debubblers used in the continuous analysis apparatus are mirror images of each other.

The proportioning pump, coils, and associated hardware were mounted on a 16 gauge painted aluminum "tray" (13 × 17 3/8 × 3-inch) one end of which is mounted to the front panel of an 14 × 18 × 12-inch Bud (Bud Radio, Inc., Willoughby, Ohio 44094) "portacab" cabinet. Mounted on the front panel (Figure 8) and exposed to the outside of the cabinet is a power switch and five fluid "Micro" valves (IN-VAL-CO, Tulsa, Oklahoma 74101) to control the input of reagents and samples. All of these snap action valves have plexiglass bodies, with stainless steel metal parts and neoprene rubber seals. The sample

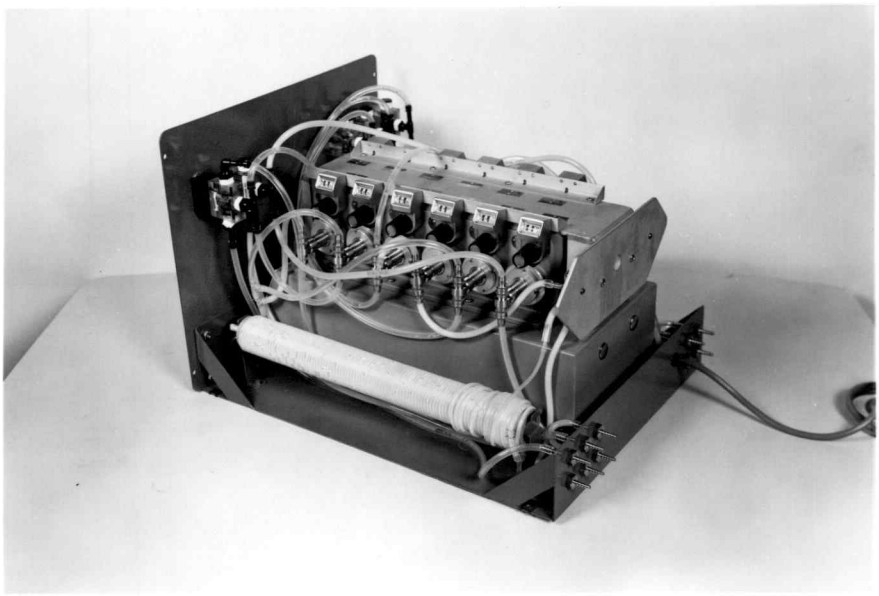

Figure 6. Chemical manipulation module with the cover removed.

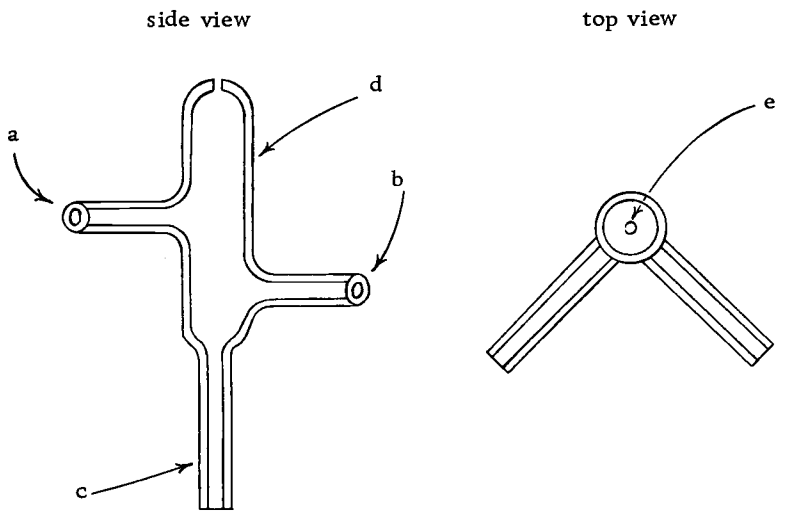

Figure 7. Diagram of debubbler.

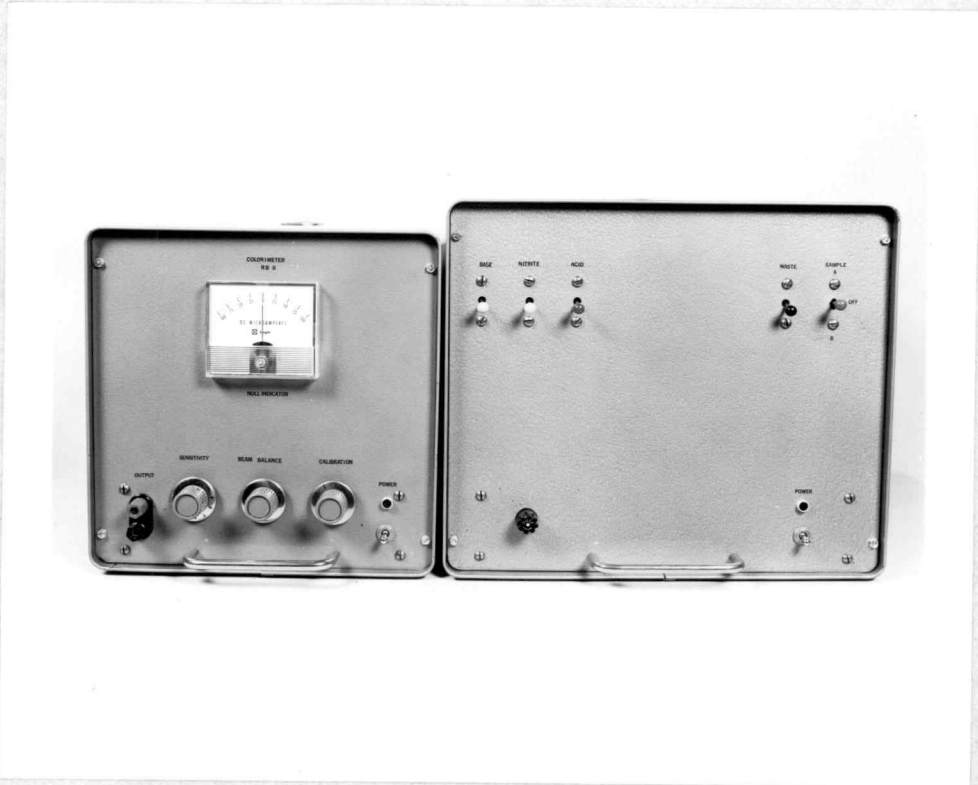

Figure 8. Front panels of the colorimeter and chemical manipulation modules.

valve is a SPDT-center off valve (type 219 F1-178N) to sample either a standard or unknown sample, while the remaining valves, controlling the nitrite, acid, base, and waste solutions, are SPDT types (316 F1-178N) with one port plugged. Plug, elbow, tee, and adaptor fittings (0.25 inch NPT to 0.131 inch tapered tubing) were polypropylene (Cole-Parmer, Chicago, Illinois 60626). All fluid connections to the pump or to the inlets were made by tygon tubing (0.0625 inch wall, 0.25 inch o.d.). Mounted on the back panel (Figure 9) of the "tray" are ten 316 stainless steel 0.125 inch tapered tubing bulkhead connectors (type 2T-BHC-2T-316) (Cajon Company, Solon, Ohio 44139). These bulkhead connectors served as input and output ports for reagents, and samples as well as for fluid connection to the colorimeter.

All of the materials used in the construction of the fluid flow system are chemically resistant to the corrosive reagents. Stainless steel, however, tends to "pit" at any air/seawater interfaces and therefore the apparatus should be thoroughly rinsed with fresh water after running saline samples.

The new fluid flow tubing material requires the reoptimization of the pump speed. A plot of the colorimeter (described in the next section) readout versus the pump speed for optimized reagents of Table A with 10 ppm Orzan A sample, is shown in Figure 10. A pump speed of 18 strokes per minute was chosen from Figure 10 to be

Figure 9. Back panels of the chemical manipulation and colorimeter modules.

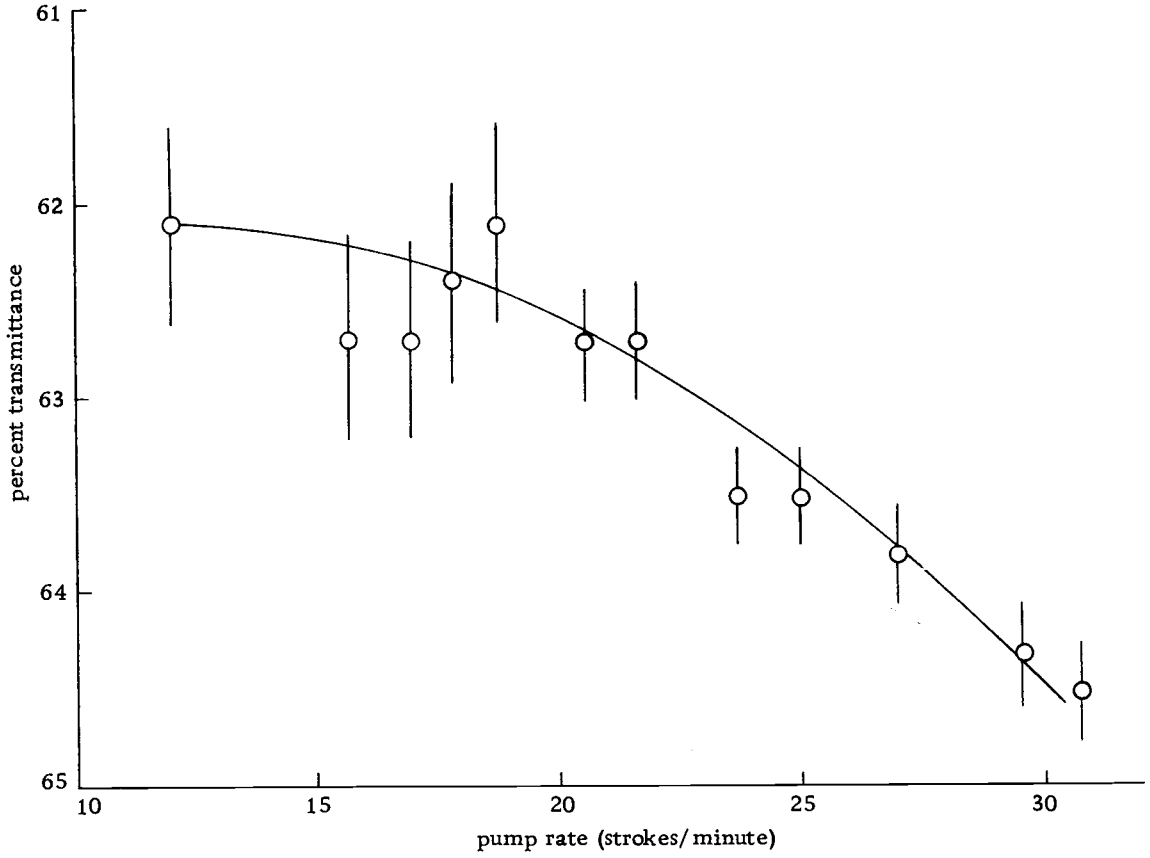

Figure 10. Dependence of color intensity on pump rate (teflon).

optimum.

Colorimeter

The determination of lignosulfonates in natural waters by the Pearl-Benson colorimetric method requires a dual beam flow-through design with long flow cuvettes. These requirements are met in the colorimeter described here.

Optics

The colorimeters optical design is based on an optical nulling technique. The arrangement of this portion of the colorimeter is shown in Figure 11. Light from a low voltage lamp type GE 1763 a (General Electric Co., Nela Park, Cleveland, Ohio 44112) operating at about 80% of its rated 6.1 volt for longer life (est. 1500 hours) is directed onto the monochromator by two first surface mirrors b (Edmund Scientific Co., Barrington, N. J. 08007). A single contact candelabra prefocus socket (Frank W. Morse Co., Boston, Massachusetts 02110) assures optical alignment from one lamp to the next.

The monochromator consists of two Bausch and Lomb (Rochester, New York 14602) multi-film light filters. The first filter c is a type 90-7 infrared blocking filter. This filter cuts off the near infrared region of the spectrum to which the photoconductive

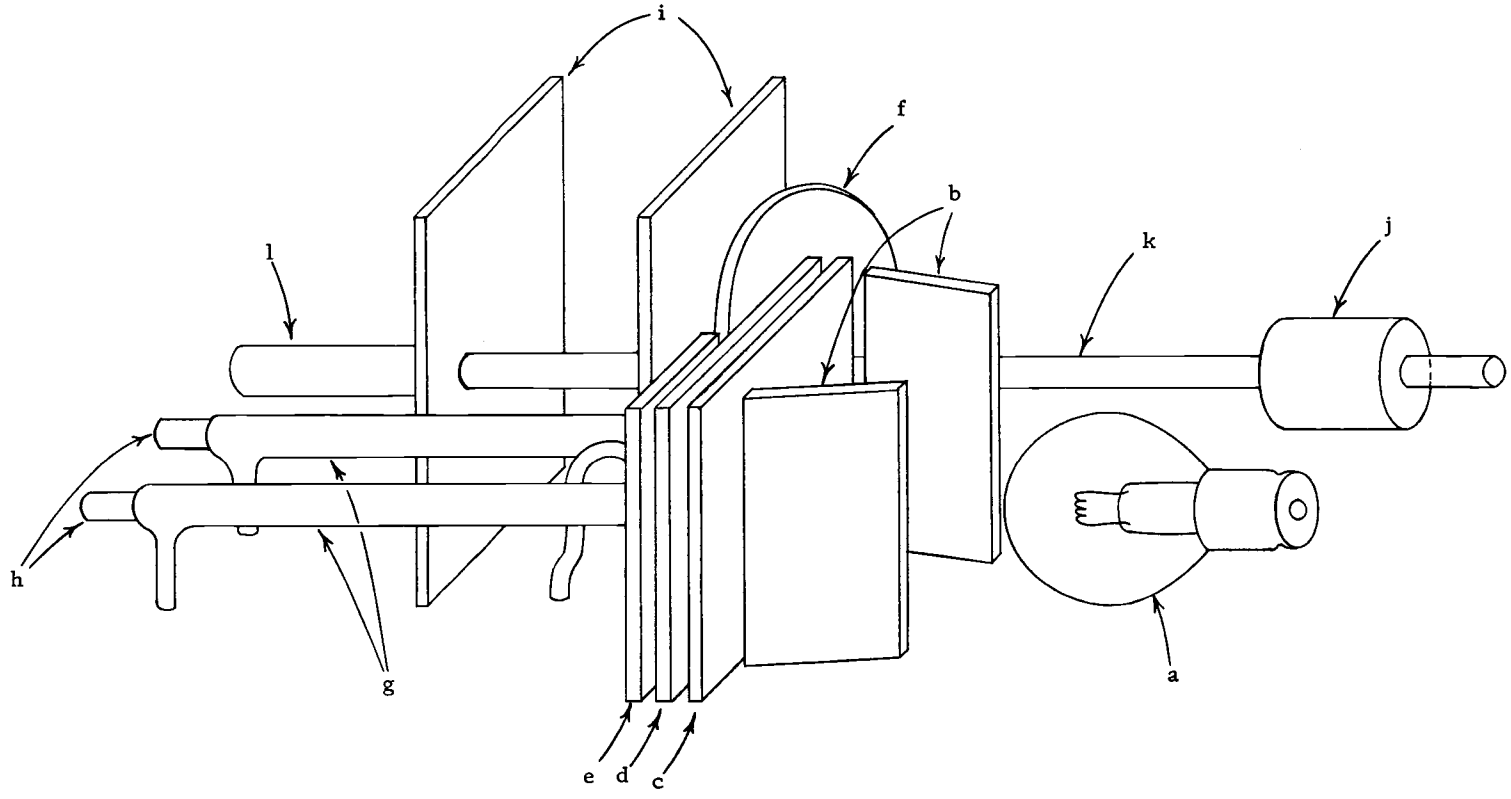

Figure 11. Colorimeter optics layout.

detectors are quite sensitive. The second filter d in the monochromator is a second order interference filter centered at 428 mμ with a 9 mμ half width (type 44-78-43). The first order band pass of this filter lies in the near infrared, necessitating the use of the infrared blocking filter. Both of these filters can be easily removed and replaced with ones of different wavelengths if desired.

Two Eastman Kodak (Rochester, New York 14650) neutral density filters are used to optically balance the sample and reference light paths. In the reference light path is placed a modified Wratten No. 96 filter of 0.30 absorbance. This filter e was made by trimming the original 2 × 2-inch gelatine filter to a 1 × 2-inch size and sealing between two glass plates of similar size. The second balancing filter is a 2.5-inch diameter inconel coated neutral density wedge, with a 1.00 absorbance unit range. The neutral density wedge f is located in the sample light path. This arrangement of balancing filters and optics permits the measurement of solutions having the effective range of -0.16 to 0.78 absorbance units (or -8.0 to +38.0 ppm Orzan A) without overrun. The portion of the range less than zero absorbance is necessary to permit adjustment of the zero point and to allow for temporarily stronger absorbance of the reference beam.

The flow cuvettes g were constructed from 7 mm pyrex glass tubing with 4 mm side arms placed as close to the ends of the cuvette body as possible (Figure 12). The window ends of the cuvette are not

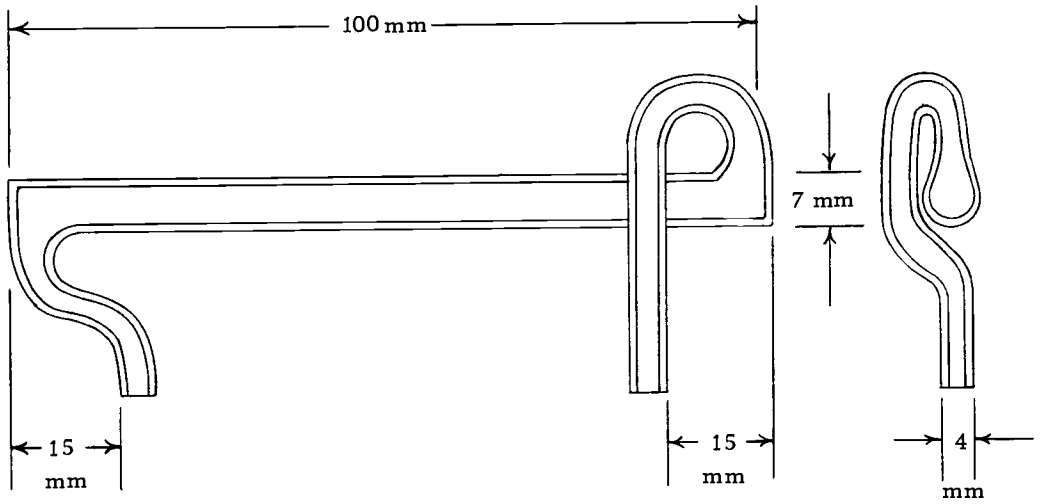

Figure 12. Diagram of flow cuvette.

optically flat. Their deviation from flatness is relatively small, however, when compared to the overall length of the cuvette. The rounding of the inside of the cuvette also helps to reduce the dead volume in the fluid flow stream.

Two clairex (New York, N. Y. 10001) CL 607L photoconductive cells, to be used as detectors h, were selected such that their resistance ratio remained nearly constant with the expected changes in light level. Type 7 cadmium sulfide photoconductors respond quickly to changes in light intensity and are reasonably sensitive to the blue portion of the visible spectrum (8). The photodetectors and the flow cuvettes were wrapped with black plastic electrical tape to minimize stray light interference.

The whole of the optical portion of the colorimeter shown in Figure 11 was housed in a $4 \times 9 \times 3$-inch, 0.25 inch thick aluminum box. Not shown in the Figure are the mounting blocks for the filters, mirrors, etc. These supports, plus the light baffles i, permit only a beam of light 15 mm thick to pass through the filters to the cuvettes. All metal parts on the interior of the box were sprayed with heat resistant flat black plant. Two 1 inch vent holes were placed immediately above and below the lamp. The box is inclined at 14° from the horizontal so that any air bubbles swept into the cuvettes, will pass on through.

The 5 to 1 speed reducer j, the connecting shaft k, and the

precision resistor 1 shown in Figure 11 are part of the readout circuit.

Electronics

The "working" portion of the colorimeter electronics is shown in Figure 13. (The list of components may be found in Table 4 located in the Appendix.) Positive and negative currents from the sample and reference detectors (R_1 and R_2) are summed by a Motorola integrated circuit operational amplifier MC 1709 CG (OA). The diodes associated with the input (D_1, D_2) and feedback (D_3, D_4) prevent input breakdown and saturation of the operational amplifier. Current from the operational amplifier is supplied to the bases of two transistors (T_1, T_2) through a 100-0-100 μa meter. The meter serves as a visual null indicator as well as a current limiting resistance for the operational amplifier. Depending upon the polarity of the operational amplifier output voltage, one of the transistors is forward biased. If the voltage is positive, T_1 will be forward biased. As T_1 becomes more conducting, the potential at the collector will drop. T_3, which was previously reversed biased by the voltage divider R_5, R_7, R_9, then becomes forward biased by the voltage divider T_1, R_7, R_9. Collector current from T_3 is fed to the gate of a TRIAC (D_5) controlling one direction of a 1 rpm reversible motor (Hurst Manufacturing Co., Princeton, Indiana). This motor then rotates the neutral density

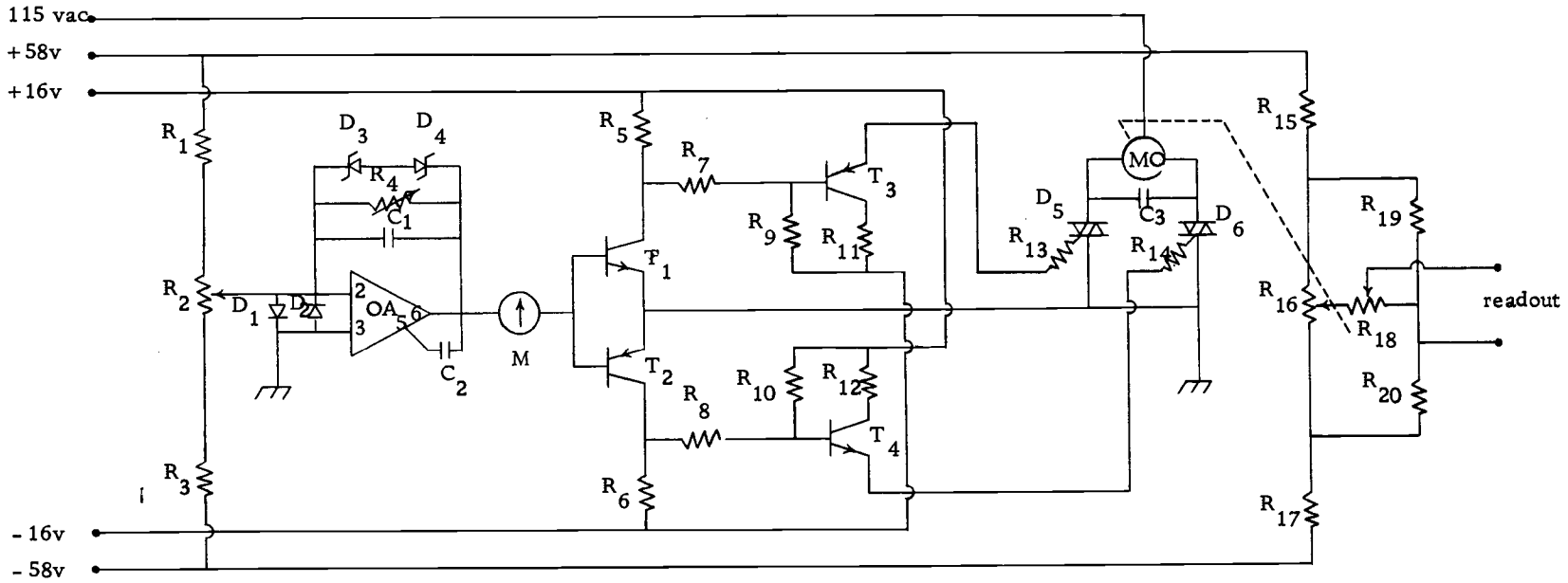

Figure 13. Colorimeter working electronics circuit.

wedge in such a manner as to balance the light falling on the two photodetectors. R_{11} and R_{13} limit the current through T_3 to the gate of the TRIAC.

The transistor switching circuit is symmetrical. Had the output voltage of the operational amplifier been negative, T_2, T_4, and D_6 would have been activated and the neutral density wedge would have rotated in the opposite direction.

A precision variable resistor R_{16} (1 in Figure 11) serves as a retransmitting slidewire indicating the position of the neutral density wedge. Since the wedge is linear in absorbance, a voltage taken from the slidewire is directly proportional to the concentration of the sample when the colorimeter is at null. A variable resistor R_{18} presents a portion of this voltage, measured between the two arms of a bridge circuit, as the readout. The bridge circuit is necessary to minimize the influence of power supply fluctuations. The resistors R_{15}, R_{17}, R_{19}, R_{20} are 100 ppm/°C precision resistors. These four resistors are wrapped together with aluminum foil and placed inside the optical box near R_{16} in order to minimize the effect of temperature drift on the readout as the colorimeter heats up. The readout presents a high output impedance (35 k maximum) and some care should be exercised in a choice of output reading devices.

The supporting power supply and associated circuitry are shown in Figure 14. (The list of components may be found in Table 4

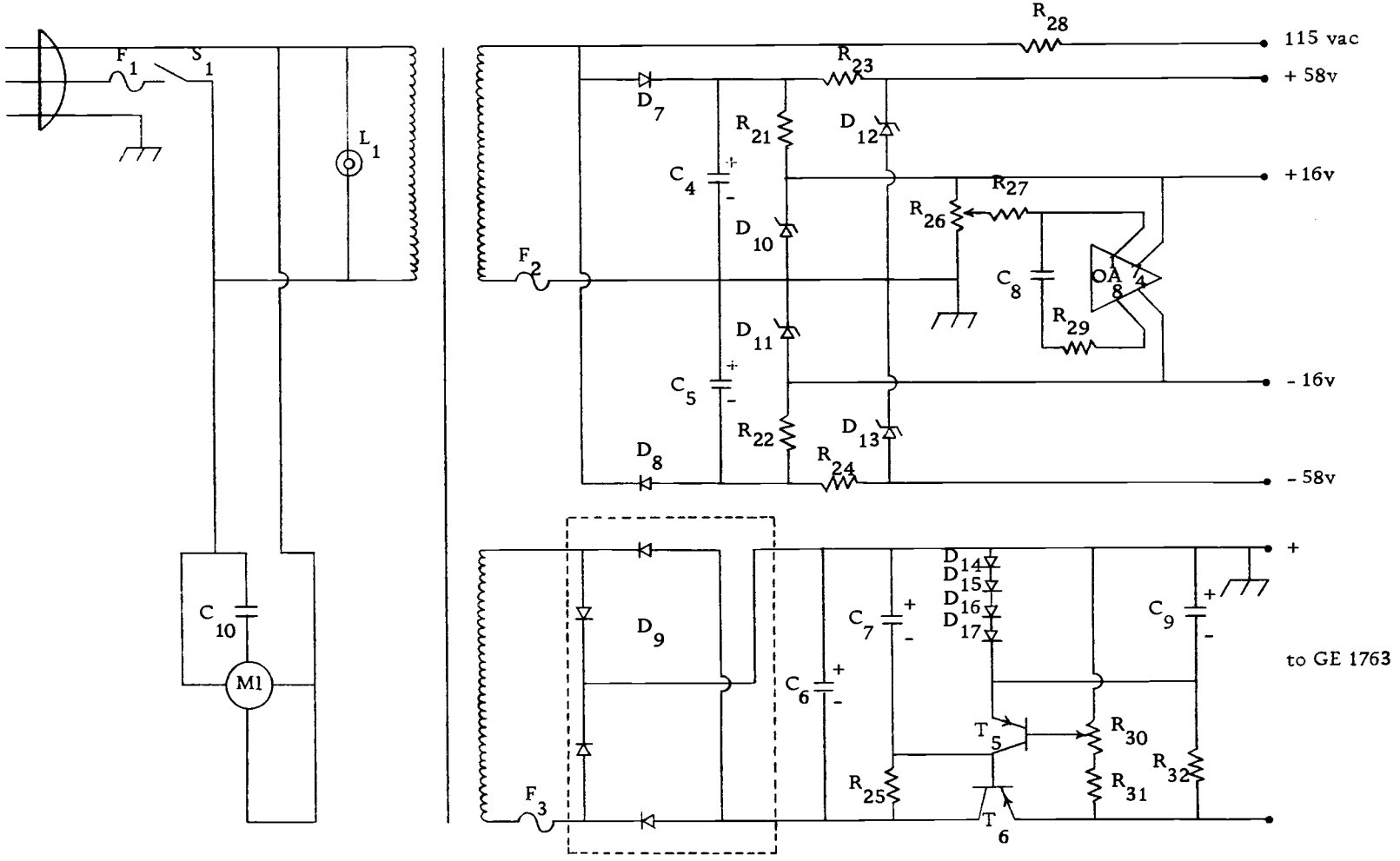

Figure 14. Colorimeter supporting electronics circuit.

located in the Appendix.) The ± 57 and ± 16 volt required for the "working" circuit are supplied by a voltage doubler power supply configuration with the center tap ground. The power supply transformer also serves as an isolation transform for the balancing motor. The appropriate supply voltages are selected by Zener diodes (D_{10}, D_{11}, D_{12}, D_{13}).

Also shown in Figure 14 is a power supply for the low voltage lamp. This supply provides stabilization against transients and permits small adjustment of the lamp intensity, through R_{31} but because of the high current drawn for the lamp (~ 4 amps), the supply provides only limited regulation. The output voltage to the lamp is furnished by T_6 operating in an emitter follower configuration. The potential at the base of T_6 is controlled by the currents passing through R_{25} and T_5, the emitter of which is tied to a reference voltage established by the diodes D_{14}-D_{17}. A negative going transient appearing at the output of the supply circuit also appears at the base of T_5 through the voltage divider R_{30}, R_{31}. This turns T_5 more "on" and causes the potential at the base of T_6 to go more positive. The emitter of T_6, following its own base voltage, goes in a positive direction reducing the effect of the negative going transient.

Most of the circuitry shown in Figures 13 and 14 is actually mounted on four plugboards. The circuit and arrangement of each card is presented in Figures 33 through 40 in the Appendix. The

remaining portion of the circuitry, the sockets for the circuit cards and the optical box are mounted on a 10 × 17 × 3-inch painted aluminum chassis (Figures 15 and 16) which in turn is mounted in a 11 × 18 × 11-inch Bud "portacab" cabinet (Figure 8). A six conductor shielded cable and microphone connectors (Amphenol series 91 six contact type) completes the electrical circuit between the optical box and the main chassis. Four controls are presented on the front panel of the cabinet: the power switch (S_1), calibration control (R_{18}), beam balance or zeroing control (R_2) and the sensitivity control (R_4).

The colorimeter possesses several characteristics which are not commonly found in a single instrument:

1. 10 cm flow cuvettes
2. dual beam operation
3. output directly proportional to concentration
4. direct current signal manipulation
5. modest cost (about $500 excluding labor)

Use of the Equipment

The circuitry of the colorimeter is designed such that operating condition will be with the controls at about midscale.

Calibration

Calibration of the readout is accomplished with the following

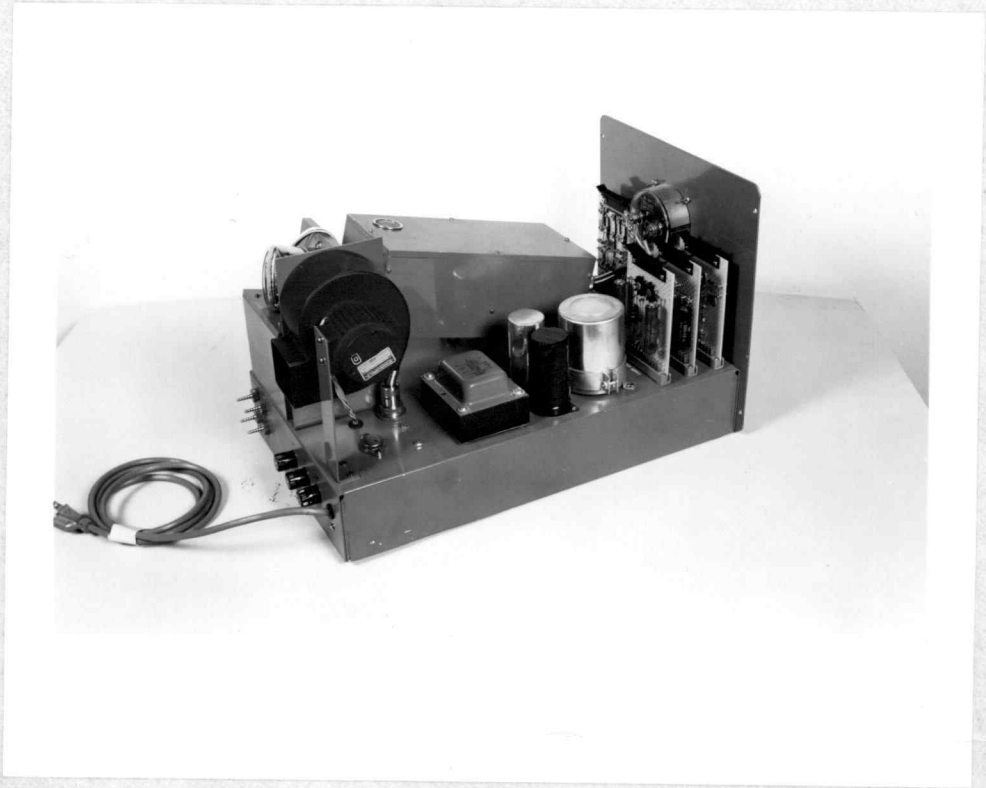

Figure 15. Colorimeter with the cover removed (above the chassis view).

Figure 16. Colorimeter with the cover removed (under the chassis view).

procedure. The pump and colorimeter are turned on and the sensitivity, beam balance and calibration controls set to midscale. After a suitable time for attainment of equilibrium for both the fluid flow system and colorimeter (about one hour), a 0 ppm SSL (or 0.0 ppm Orzan A) standard sample is submitted to the apparatus for analysis. Care should be taken to see that the standard matrix is as close as possible to that of the samples to be analyzed. While the colorimeter is responding to this standard, the beam balance control R_{18} is adjusted until the readout voltage is 0 mv. A 100 ppm SSL (or 10.0 ppm Orzan A) standard is then submitted for analysis. In this case the calibration control R_2 is adjusted until the readout voltage is 100 mv. Again the 0 ppm SSL standard is submitted for analysis and the beam balance control adjusted for 0 mv output. The readout of the colorimeter in millivolts should then correspond to the SSL concentration in parts per million. Variation of the calibration control effectively changes the slope of the calibration curve. This is advantageous since the absorptivity of the method is known to change in going from fresh to seawater matrices as reported earlier.

Figure 17 presents the output of the colorimeter versus input concentration after such a calibration procedure. The analytical curve is linear and possesses a standard deviation of 1.8 ppm SSL. The delay time and response time (Figure 18) for the apparatus are observed to be 3.6 and 6.5 minutes, respectively, at pump speeds

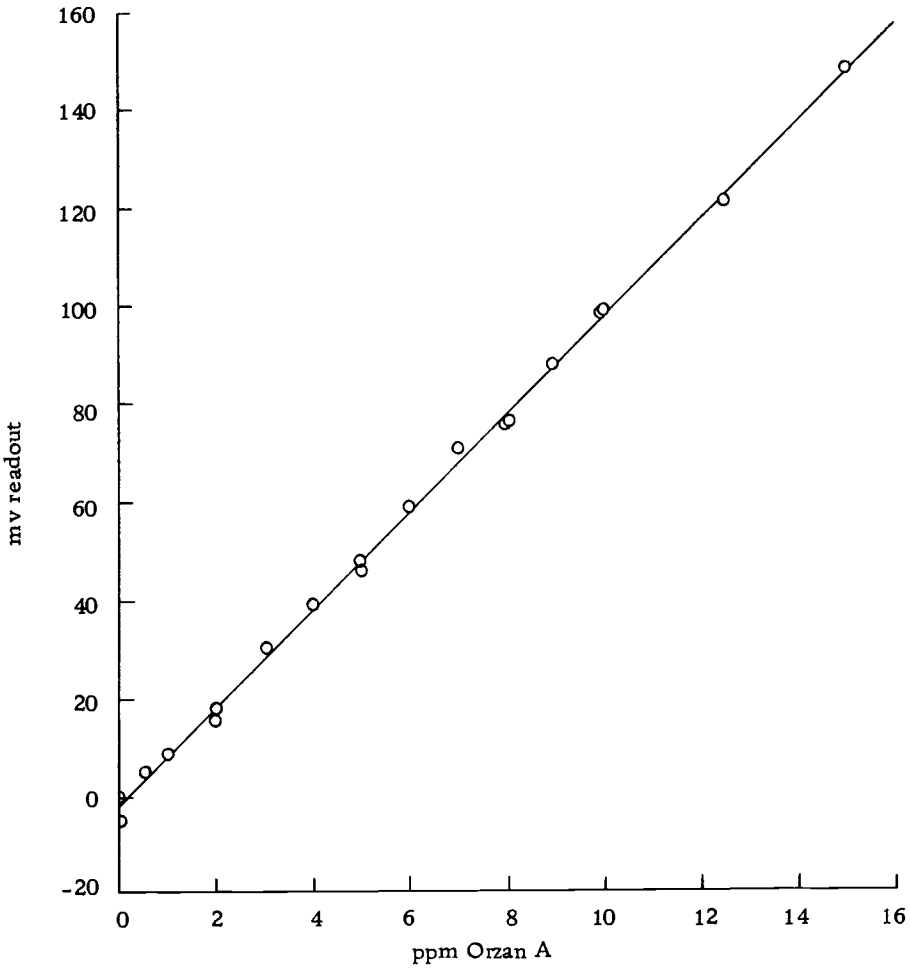

Figure 17. Colorimeter calibration curve.

of about 18 strokes per minute. This compares with a readout time of about 30 minutes for the standard method.

Determination in Natural Waters

An attempt was made to estimate the level of SSL in the Willamette River water samples used earlier in the discussion of clarification. When the sample, which had settled overnight, was submitted for analysis, to the chemical manipulation and colorimeter modules, the colorimeter indicated 51 ppm. The same sample, when analyzed by a manual method equivalent to the optimized procedure and measured by a Beckman DB spectrophotometer with 1.0 cm cuvettes, read less than one tenth of that value. When known amounts of Orzan A were added to the river water and these samples again submitted to the apparatus for analysis, the readout was still observed to have a slope of one millivolt per part per million SSL.

It would appear that the natural water sample, with its background absorbance equivalent to over 40 times that produced by its SSL content, has brought about an offset in the colorimeter of about 50 ppm. Such an offset would manifest itself if the detectors were not well matched with regard to resistance change per light level change.

The operator has four choices then if he wishes to estimate the SSL level in turbid samples. He can 1) filter the sample using

appropriately small pore size in order to remove interferences, but then suffers the risk of also filtering out the lignosulfonates. He can 2) calibrate the colorimeter using standard solutions which have a background absorbance equivalent to the natural water samples under investigation. He can 3) select a better matched pair of photo-conductive cell detectors for the absorbance levels involved. Or he can 4) return to running the Pearl-Benson determinations manually.

It is clear that the equipment described earlier in this section is subject to many of the same problems appearing in manual methods for natural water samples. While it may not be a panacea for these ills, it does represent an improvement in the ability to perform similar types of analysis under less severe conditions.

SIMULATION OF CONTINUOUS ANALYSIS RESPONSE

If a step change in concentration is submitted to the input of a continuous analysis apparatus, an immediate step change is not observed at the output. It takes some period of time, the response time, before the output signal reflects the new concentration. The response time of continuous analysis apparatus to a step change input can be divided into two parts as shown in Figure 18. The delay time t_d is the time required, after initiation of a step change input, for the detector to begin its response to the samples presence. The transition time t_t is the time required for the detector, once it has begun to respond to the sample, to reach an equilibrium value indicative of the concentration of the step input. The delay time and the transition time are attributable to fluid transport and unintentional mixing processes.

Several workers have examined the nature of this response. Chaney (7) has applied the parameters of fluid mechanics to the air segmented fluid flow commonly used in continuous analysis. Larson, Sanderson, and co-workers (19, 22), observing the transition curve of some air pollutant monitors, find that much of the sigmoidal transition curve can be fitted with an exponential equation of the form:

$$m_a = m_f - (m_f - m_o)\, e^{-t/T} \qquad (1)$$

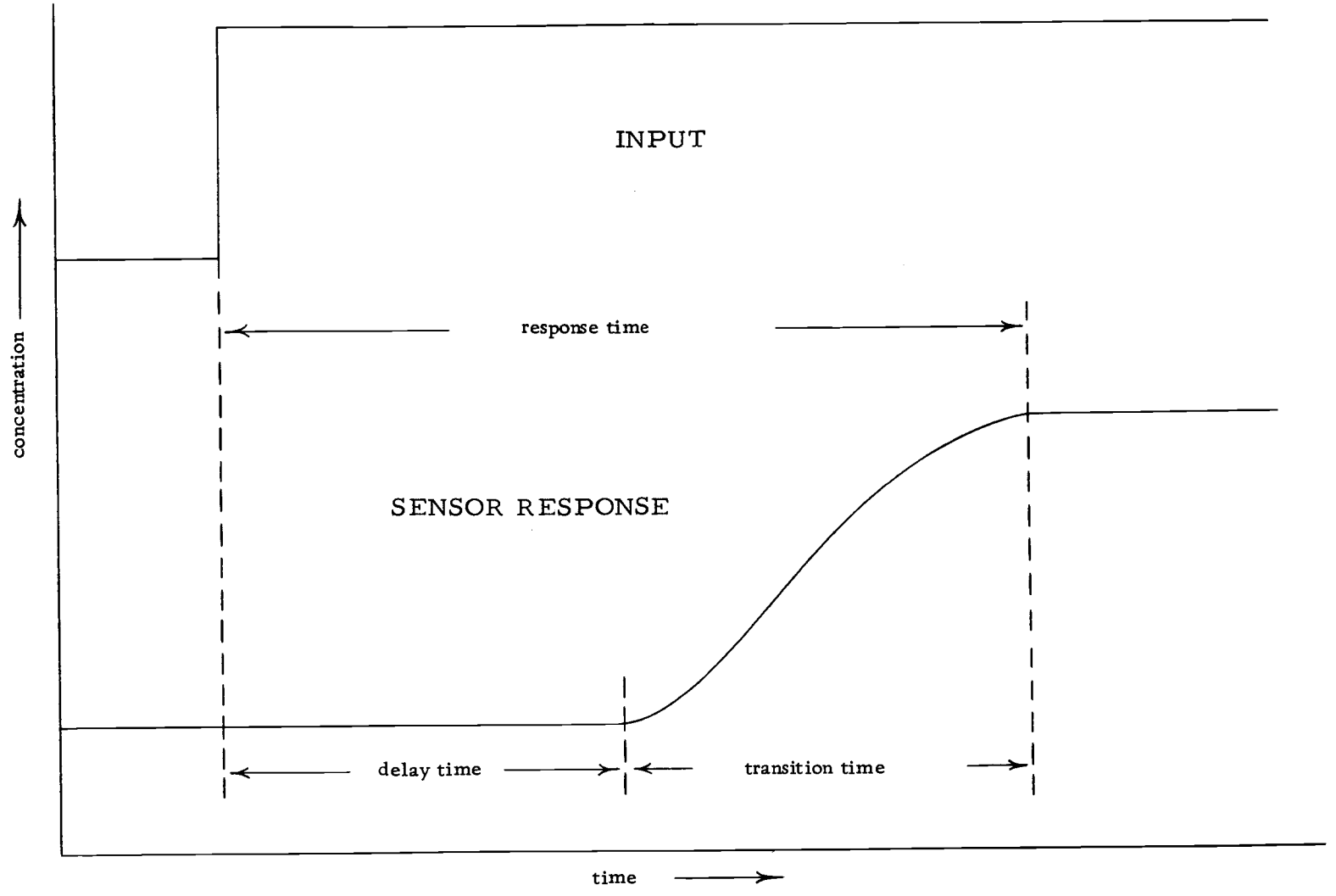

Figure 18. Continuous analysis response to a step change.

where m_a is the apparent concentration at time t, m_f is the final concentration for a step change input, m_o is the concentration before initiation of the step change and T is a time constant characteristic of the particular apparatus. Thiers and co-workers (33), using equipment commonly employed in continuous analysis, observed a similar response.

The fitting of much of the transition curve by Equation 1 indicates a basically exponential process with some perturbations of that process to produce the "knee" of the sigmoidal transition curve. It is observed that such perturbations can be accounted for by inclusion of additional exponential terms in the response equation.

A continuous analysis apparatus may be thought of, then, as a "black box" with input and output terminals such that a step change at the input terminals results in a sigmoidal change at the output at some later time.

Analog

An electronic circuit which has a simple exponential response to a step change input is shown in Figure 19. If a Kirchoff loop equation is written for the circuit, using lower case letters to represent time varying functions, the output (apparent) signal v_a is related to the input signal v_i by:

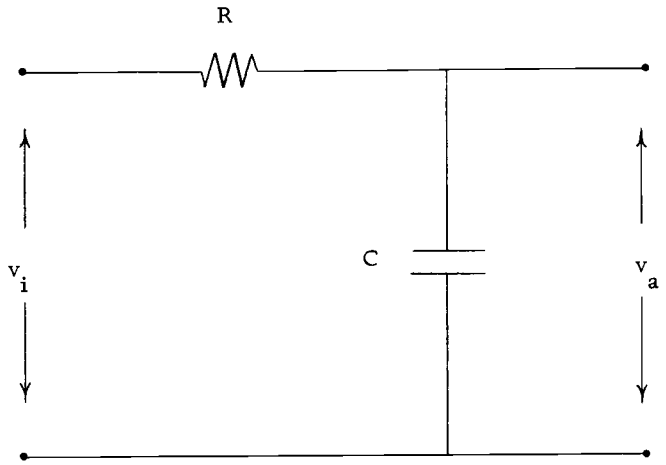

Figure 19. Exponential analogy circuit.

$$v_i - iR - v_a = 0 \tag{2}$$

Noting that the current i is proportional to the rate of charging of the capacitor, gives:

$$v_i - RC\dot{v}_a - v_a = 0 \tag{3}$$

Expressing this equation in the s - domain and letting $T = RC$, yields the familiar LaPlace transform for a simple exponential device:

$$V_i - T[s V_a - v_a(0)] - V_a = 0 \tag{4}$$

$$V_i - T s V_a - V_a = 0 \tag{5}$$

and

$$\frac{V_a}{V_i} = \frac{1}{1 + T s} \tag{6}$$

where upper case variables refer to the LaPlace transforms of the respective lower case functions.

If a number of units, n, each possessing a transfer function of the form of Equation 6, were to be placed in series, the overall transfer function would have the form:

$$\frac{V_a}{V_i} = \frac{1}{(1 + T_1 s)} \times \frac{1}{(1 + T_2 s)} \times \ldots \times \frac{1}{(1 + T_n s)} \tag{7}$$

This transfer function yields a response analogous to the transition curve of a continuous analysis system. The cascading of simple R C networks does not, unfortunately, lead directly to this form due to the

inevitable loading of earlier R C networks by those that follow (18, p. 1-6). A circuit possessing a transfer function of the form of Equation 7, with $n = 2$, but which permits sufficient current to be drawn to prevent loading, can be synthesized using operational amplifiers (6). The circuit, shown in Figure 20, has a transfer function given by:

$$\frac{V_a}{V_i} = \frac{R_4 R_6}{R_3 R_5} \frac{1}{(1 + R_4 C_3 s)(1 + R_6 C_4 s)} \tag{8}$$

Letting $R_3 = R_4$, $R_5 = R_6$, $T_1 = R_4 C_3$ and $T_2 = R_6 C_4$ yields a transfer function of the appropriate form. The assignment of the feedback loop of OA1 to generate T_1 is arbitrary since the transfer function would be of the same form if it were assigned to OA2.

If a transfer function of the form of Equation 7 is used to represent the distortion of the step change input into the sigmoidal shaped output observed, and if a term is added to such a transfer function to account for the delay time, then the "black box" or mathematical model representing the continuous analysis apparatus can be represented by:

$$\frac{M_a}{M_i} = \frac{e^{-t_d s}}{(1 + T_1 s)(1 + T_2 s) \cdots (1 + T_n s)} \tag{9}$$

where the electrical signals have been replaced with apparent and input concentration terms M_a and M_i. Again the upper case

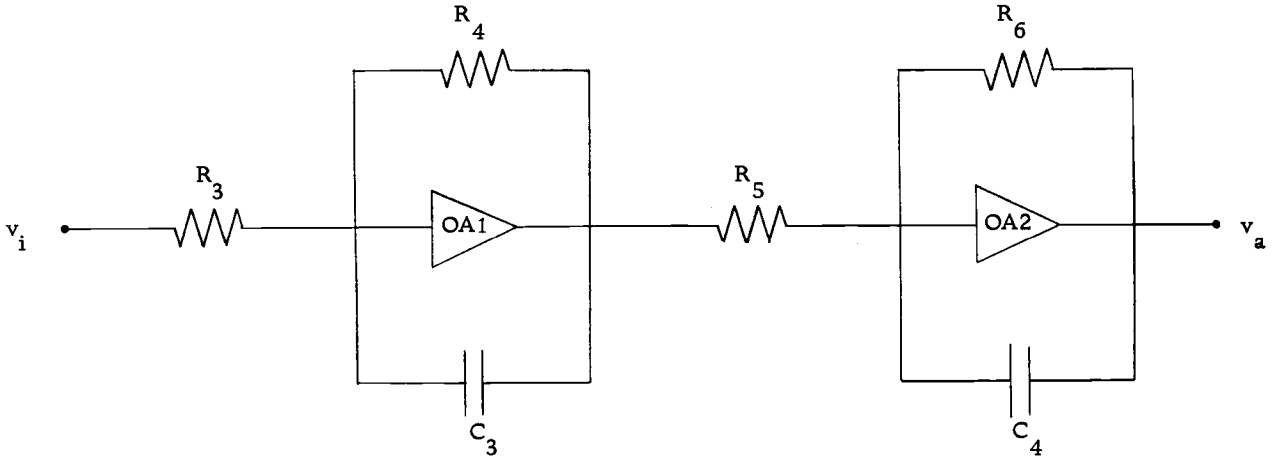

Figure 20. Continuous analysis response simulator.

variable refer to the LaPlace transforms of the time varying signals.

If Equation 9 is solved, by the method of partial fractions, using a step change input at $t = 0$, the response of the mathematical model as a function of time is given by:

$$m_a = m_f - (m_f - m_o)\left[K_1 e^{-(t - t_d)/T_1} + K_2 e^{-(t - t_d)/T_2} + \cdots + K_n e^{-(t - t_d)/T_n}\right] \quad (10)$$

When all of the time constants are equal, the kth coefficient of Equation 10 is given by:

$$K_k = \frac{(t - t_d)^{(k - 1)}}{(k - 1)!\ T^{(k - 1)}} \quad (11)$$

If the time constants are not equal, the coefficients of Equation 10 are of the form:

$$K_1 = \frac{T_1^{(n - 1)}}{(T_1 - T_2)(T_1 - T_3) \cdots (T_1 - T_n)} \quad ;$$

$$K_2 = \frac{T_2^{(n - 1)}}{(T_2 - T_1)(T_2 - T_3) \cdots (T_2 - T_n)} \quad ; \text{ etc.} \quad (12)$$

A particularly useful form of Equation 10 results when $n = 2$ and $T_1 \neq T_2$:

$$m_a = m_f - (m_f - m_o)\left[\frac{T_1}{T_1 - T_2} e^{-(t - t_d)/T_1} - \frac{T_2}{T_1 - T_2} e^{-(t - t_d)/T_2}\right] \quad (13)$$

This equation fits the response of continuous analysis apparatus whose

total fluid flow length is short. For longer fluid systems, values of n greater than two must be taken.

If there is sufficient difference in magnitude between the larger time constant T_1 and the smaller time constant T_2 in Equation 13, then after some period of time the exponential term involving T_2 will have decayed away and Equation 13 could be rewritten in logarithmic form.

$$\log \frac{(m_f - m_a)}{(m_f - m_o)} = \frac{-(t - t_d)}{2.30\ T_1} + \log \frac{T_1}{T_1 - T_2} \qquad (14)$$

The time constants T_1 and T_2 then can be evaluated from a semilog plot of $(m_f - m_a)/(m_f - m_o)$ versus t, letting $t_d = 0$ and plotting only the transition curve. T_1 is obtained from the slope γ of the straight line portion of such a plot and T_2 from the intercept $B \equiv \log A$.

$$T_1 = \frac{0.434}{\gamma} \qquad (15)$$

$$T_2 = \frac{T_1\ (A - 1)}{A} \qquad (16)$$

Experimental

The continuous analysis apparatus, reagents and methodology used in this theoretical investigation, were the same as the optimized continuous analysis procedure of the chemical optimization chapter.

In order to better understand the real continuous analysis system, experiments were carried out on a model of such a system, illustrated in Figure 20. This was accomplished on a Burr-Brown Model 600 Analog Simulator (Burr-Brown Research Corporation, Tuscon, Arizona). Step, ramp, and sinusoidal inputs are normally used in a feedback control theory to evaluate the performance of a system. Such inputs were used in this investigation.

If a step change in concentration is submitted to the continuous analysis apparatus and the resultant transition curve plotted as the $\log (m_f - m_a)/(m_f - m_o)$ versus the time after the observable beginning of the transition curve, a curve such as that shown in Figure 21 is obtained. The straight line portion of such a curve can be expressed by the equation:

$$\log \frac{(m_f - m_a)}{(m_f - m_o)} = \gamma t + B \qquad (17)$$

where, as earlier, γ is the slope of the line and B is the intercept. Solving Equation 17 for γ and substituting this value into Equation 15:

$$T_1 = 0.434\ t \left[\log \frac{(m_f - m_a)}{(m_f - m_o)} - B \right]^{-1} \qquad (18)$$

Taking from Figure 21 the intercept $B = \log 2.10$ (hence $A = 2.10$) and one other point on the straight line (say $\log (m_f - m_a)/(m_f - m_o) = \log 0.11$ at $t = 2.40$ minutes), the time constants of $T_1 = 49$ seconds

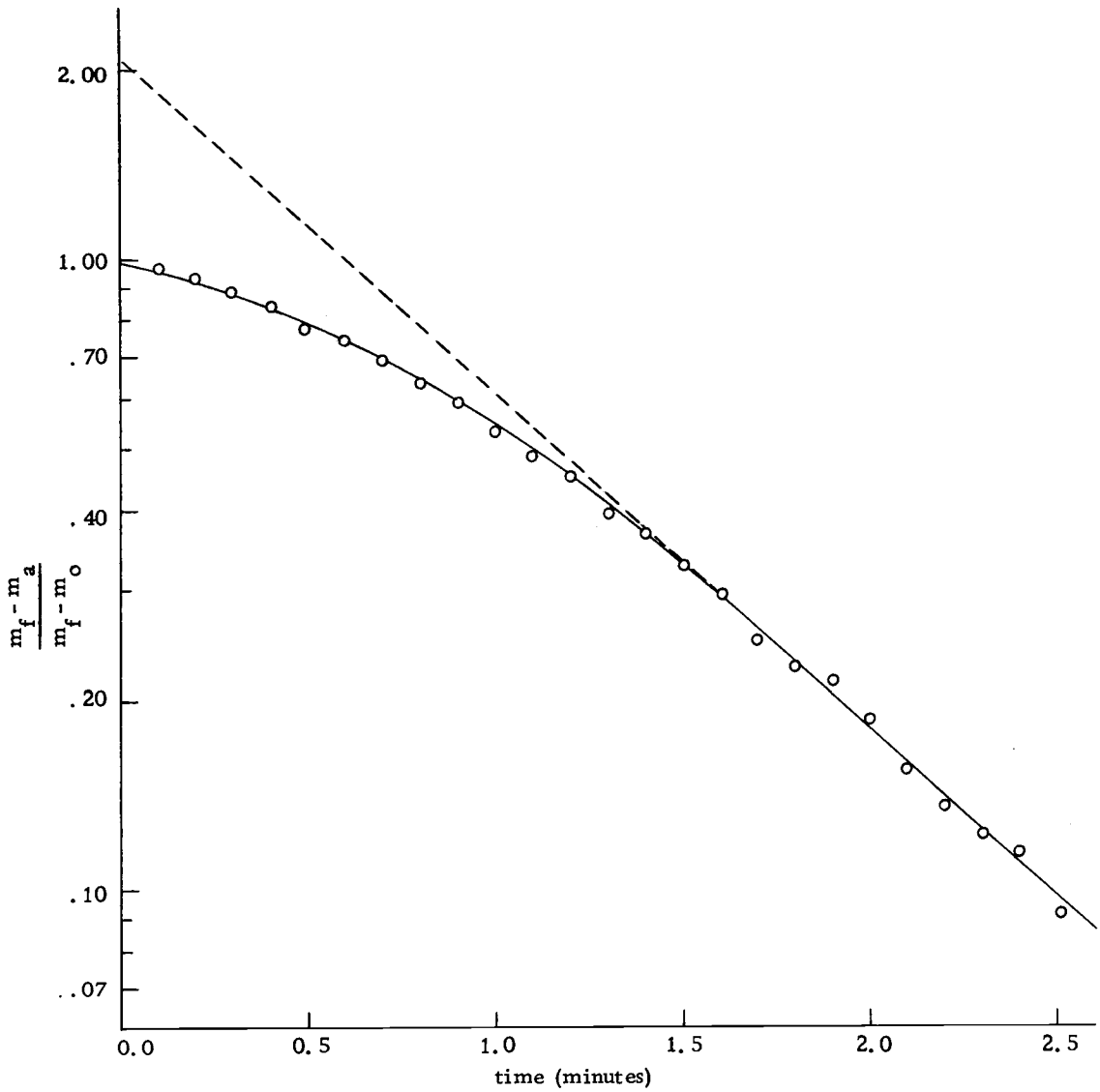

Figure 21. Semilog plot of transition curve.

and $T_2 = 26$ seconds were obtained from Equations 18 and 16.

If step changes in concentration are submitted to the continuous analysis apparatus, and these step changes are maintained for varying lengths of time, a family of transition curves, shown in Figure 22, is obtained. Simulation of the time constant ratio $T_2 : T_1 = 0.53$, under similar input conditions, produced a family of transition curves which was qualitatively but not quantitatively like that of the real system. The simulated response indicated that a short period of time (approximately 15% of T_1) occurs after the initiation of the experiment but before any change in the output is observed. This so called capacitive delay corresponds to a period of time in the response of a $n = 2$ system in which the change in the output is so small as to be indiscernible to the observer. When this capacitive delay time was included in the transition curve of the real system (Figure 21) and T_2 recalculated, a time constant ratio of 0.60 was obtained. Figure 23 shows the family of transition curves for a simulated system of $T_2 : T_1 = 0.61$. A comparison of Figures 22 and 23 shows that the simulation model reliably predicts the real systems response to step change input of varying duration.

If a step input is submitted to a simulation model containing a number of capacitive elements having the transfer function of Equation 6, all of equal time constants, a family of transition curves, such as that shown in Figure 24, is developed. As n becomes larger a

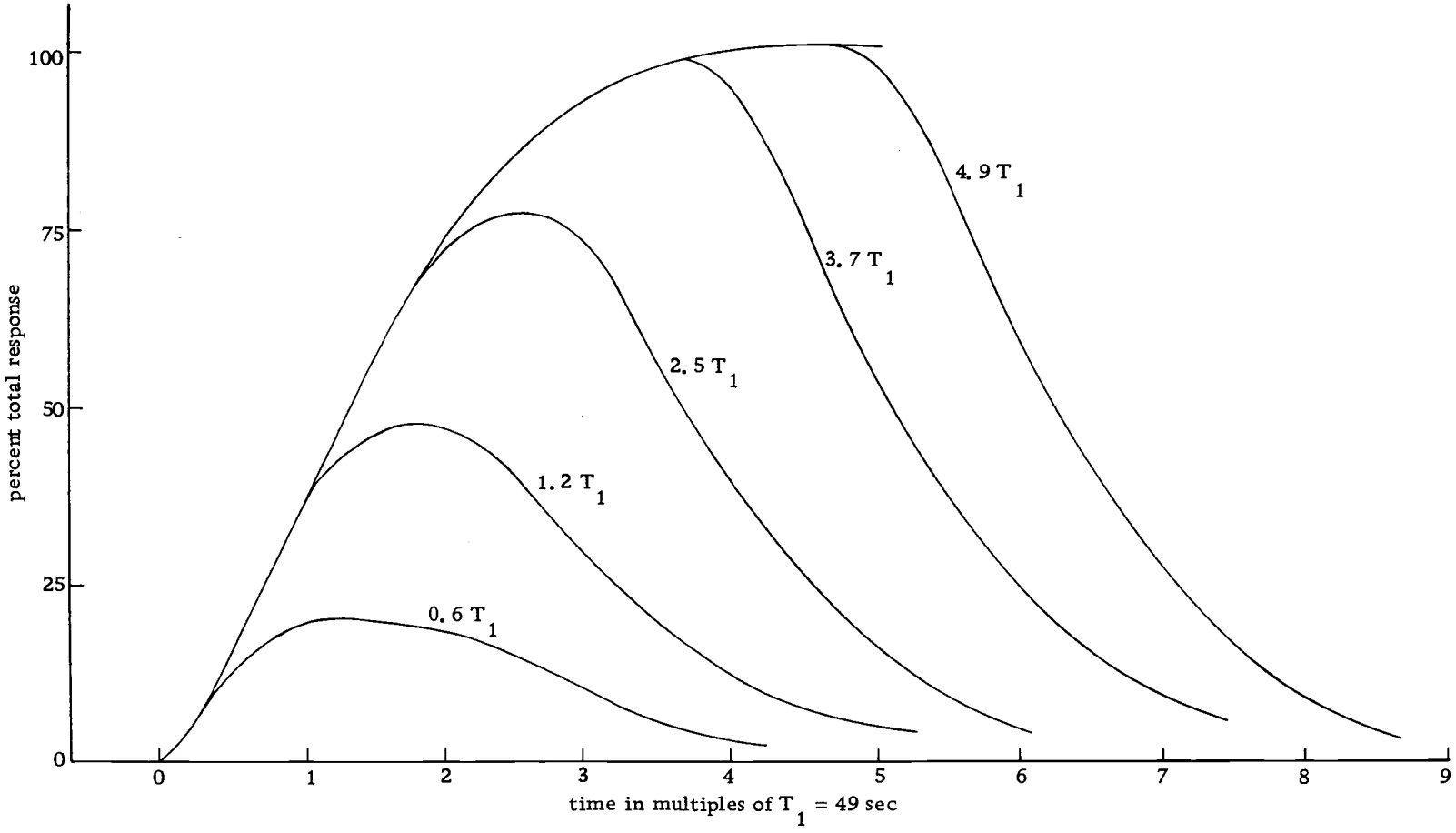

Figure 22. Continuous analysis transition curves for step inputs of various duration.

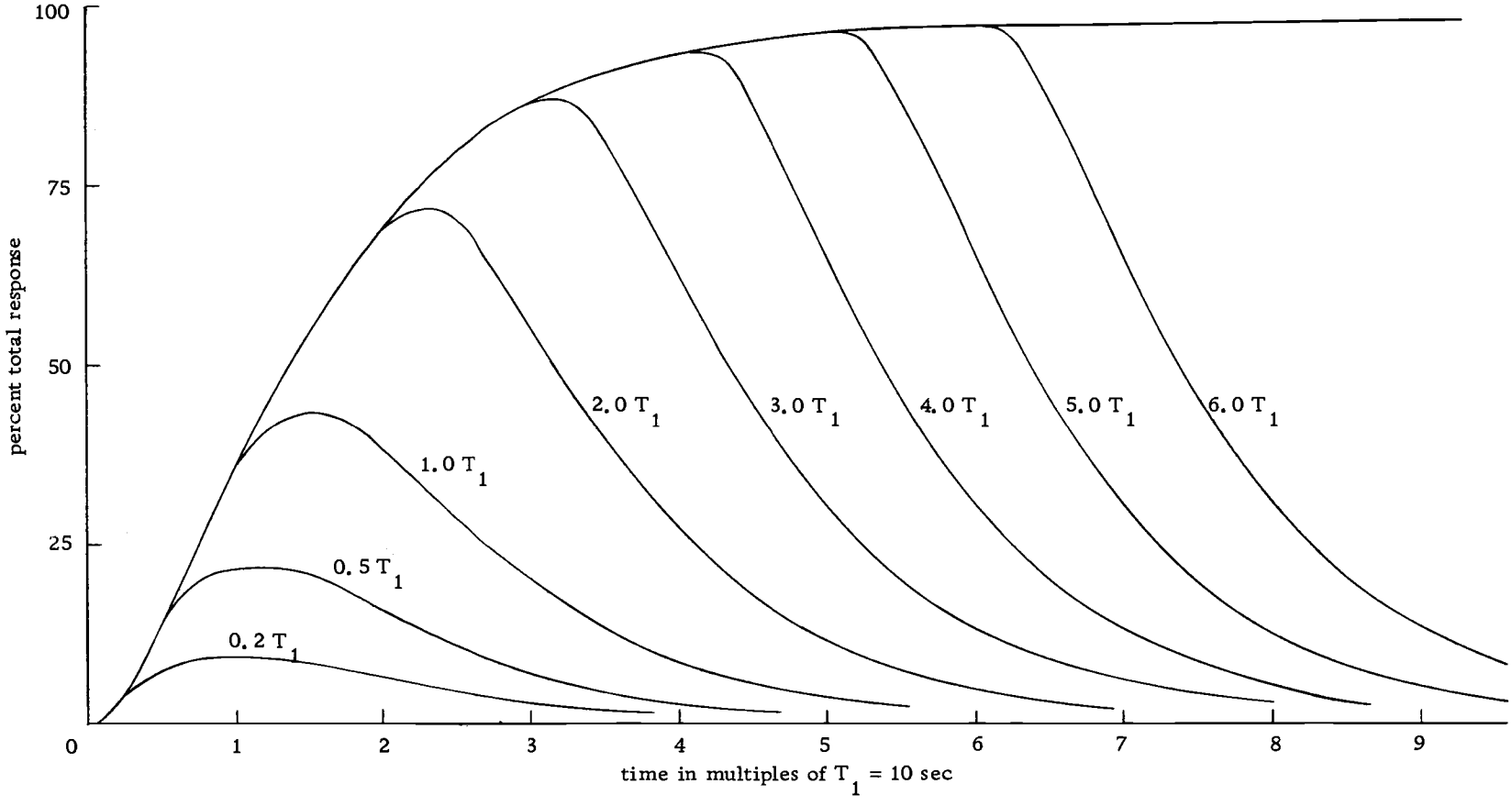

Figure 23. Simulated transition curves for step inputs of various duration.

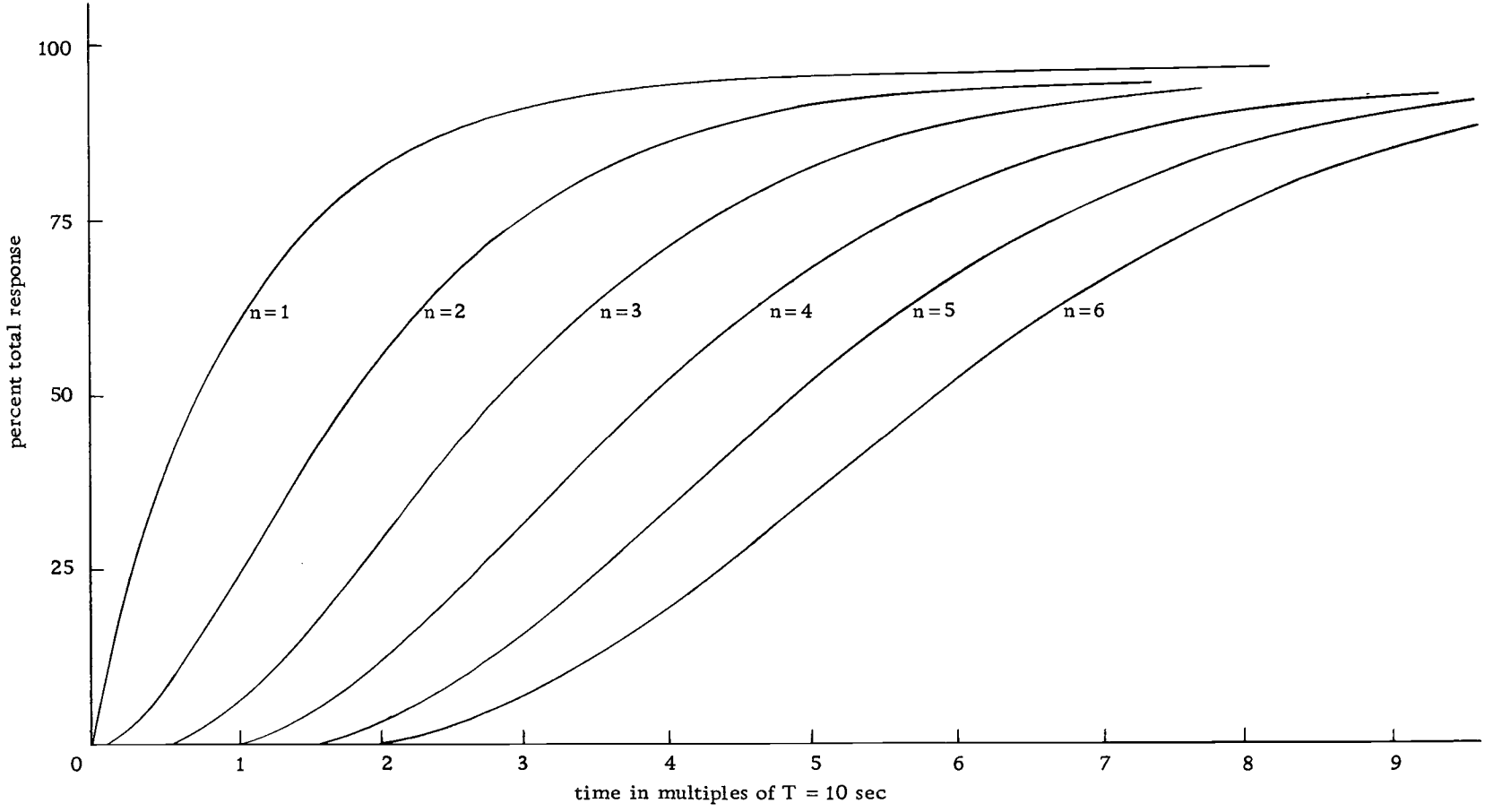

Figure 24. Simulated transition curves for various values of n.

number of effects are observed; 1) the transition curve becomes more sigmoidal in nature, 2) the equilibrium value is reached more slowly, and 3) evidence of the transition itself occurs later. The latter observation indicates that the delay time is composed of at least two parts; a pure transportation delay and a capacitive delay.

If a step input is submitted to a model containing only two such capacitive elements, in which the time constants are not equal, a family of curves is observed (Figure 25) which is qualitatively similar, but less pronounced, than the multiple n case. Clearly, from Figure 25, only time constants of the same order of magnitude effect the shape of the transition curve.

Ramp and sinusoidal changes in concentration are harder to obtain and the real system was not evaluated using these inputs. However electrical input signals of this nature can be readily synthesized and were used to evaluate the model and to predict the response of the real system to such inputs.

The response of the model ($n = 2$; $T_2 : T_1 = 0.61$) to a ramp input is shown in Figure 26. After an initial transient period, the simulator faithfully follows the ramp input but is displaced from that input by a constant lag time.

The response of a system to a ramp input permits the evaluation of one of the "figures of merit" of a dynamic system. The rate-of-change or velocity constant K_v is related to v, the slope of

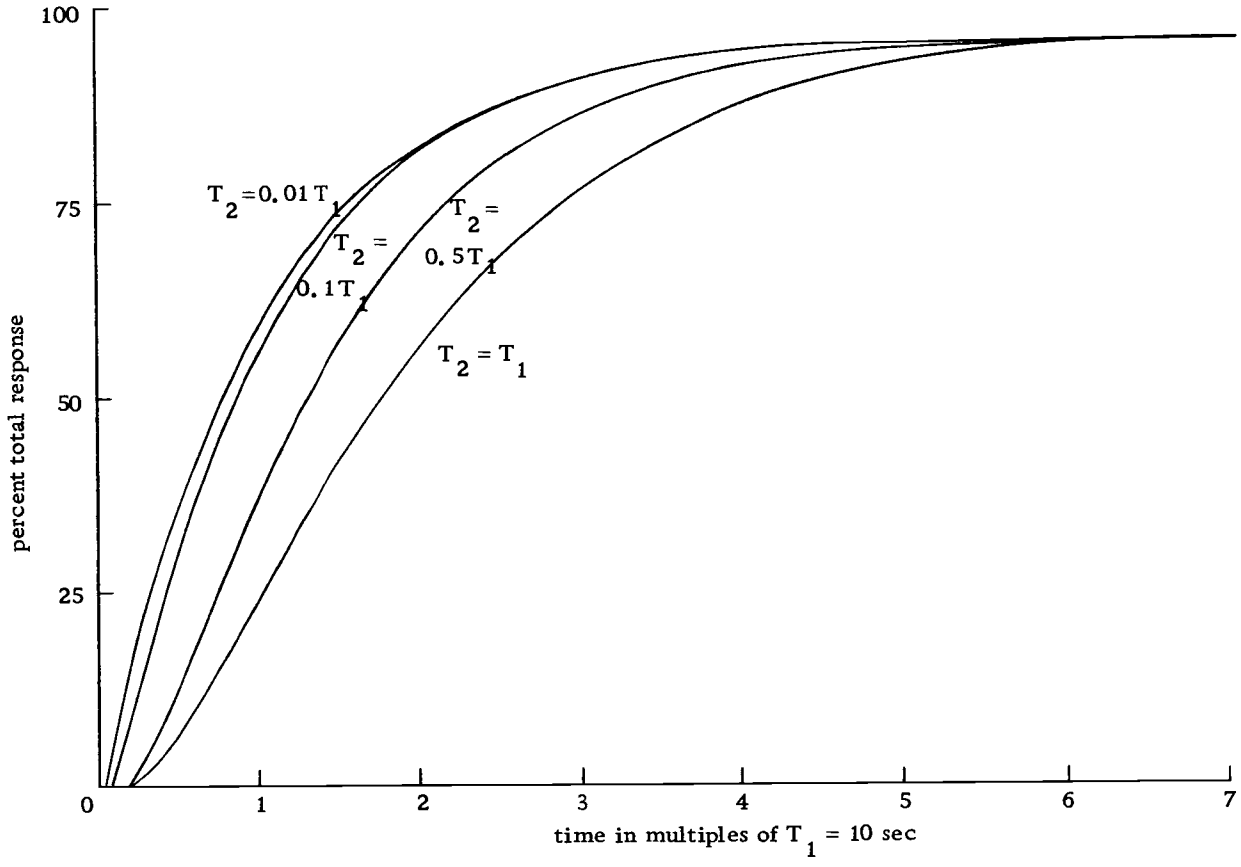

Figure 25. Simulated transition curves for various time constant ratios.

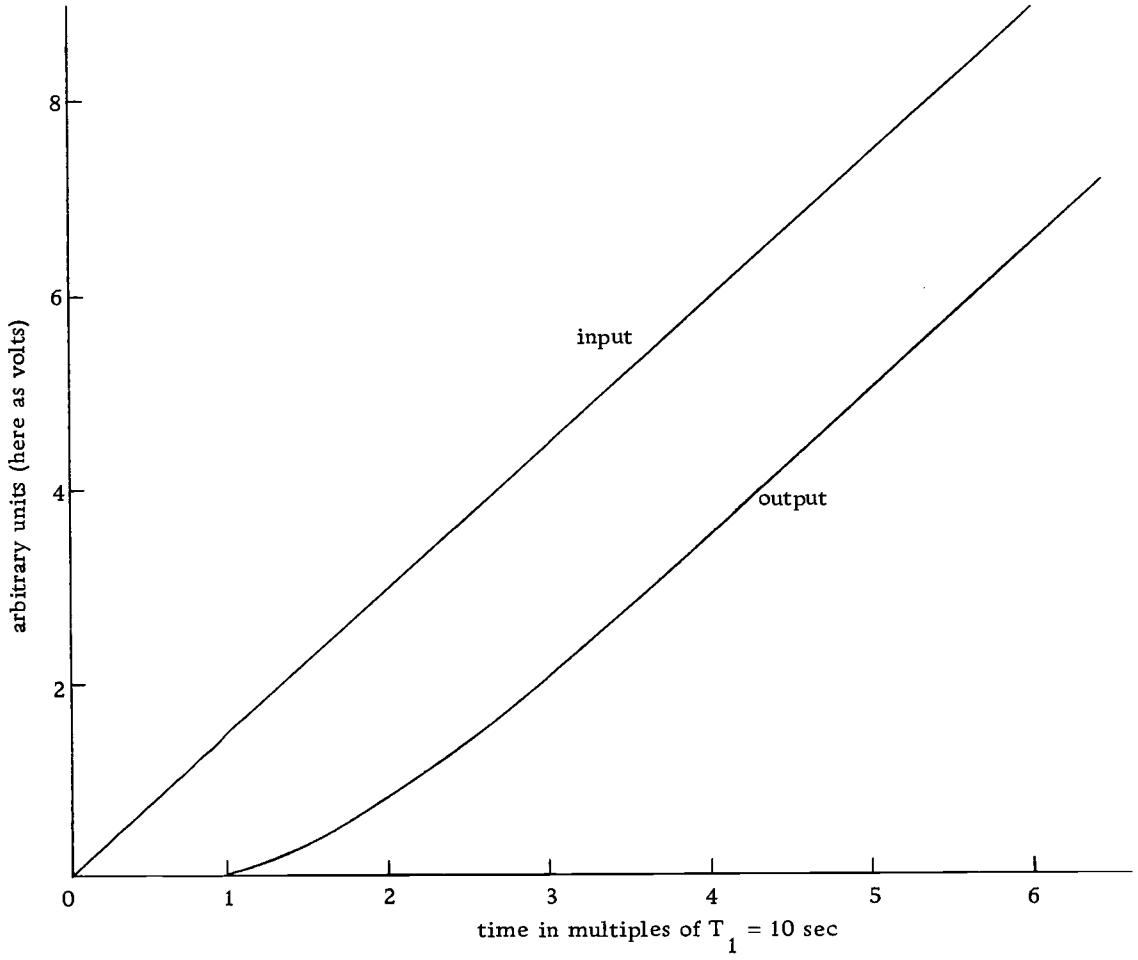

Figure 26. Simulated transition curve for a ramp input.

the ramp as a function of time, and to ϵ_v, the error between the ramp input and the system output at any time after the steady state condition is obtained, by the equation: (23, p. 83-85)

$$K_v = \frac{\nu}{\epsilon_v} \tag{19}$$

Equation 19 indicates that a maximum value of K_v is necessary for a minimum error.

The response of the model ($n = 2$; $T_2 : T_1 = 0.61$) to sinusoidal inputs at two frequencies is shown in Figure 27. After an initial transient period of several time constants, the output of the simulator reaches a steady state condition. The amplitude of the output signal is observed to decrease with increasing frequency. The magnitude of the gain G (ratio of output to input amplitude) can be estimated by: (26, p. 183)

$$|G| = \left[\frac{1}{(1 + \omega^2 T_1^2)(1 + \omega^2 T_2^2)} \right]^{1/2} \tag{20}$$

The angular velocity ω is, of course, related to the period τ by $\omega = 2\pi/\tau$ The phase angle ϕ, relating the complex output signal to the complex signal, decreases with increasing frequency, but at a rate slower than the decreasing period. The magnitude of the phase angle can be estimated by: (27, p. 41-42)

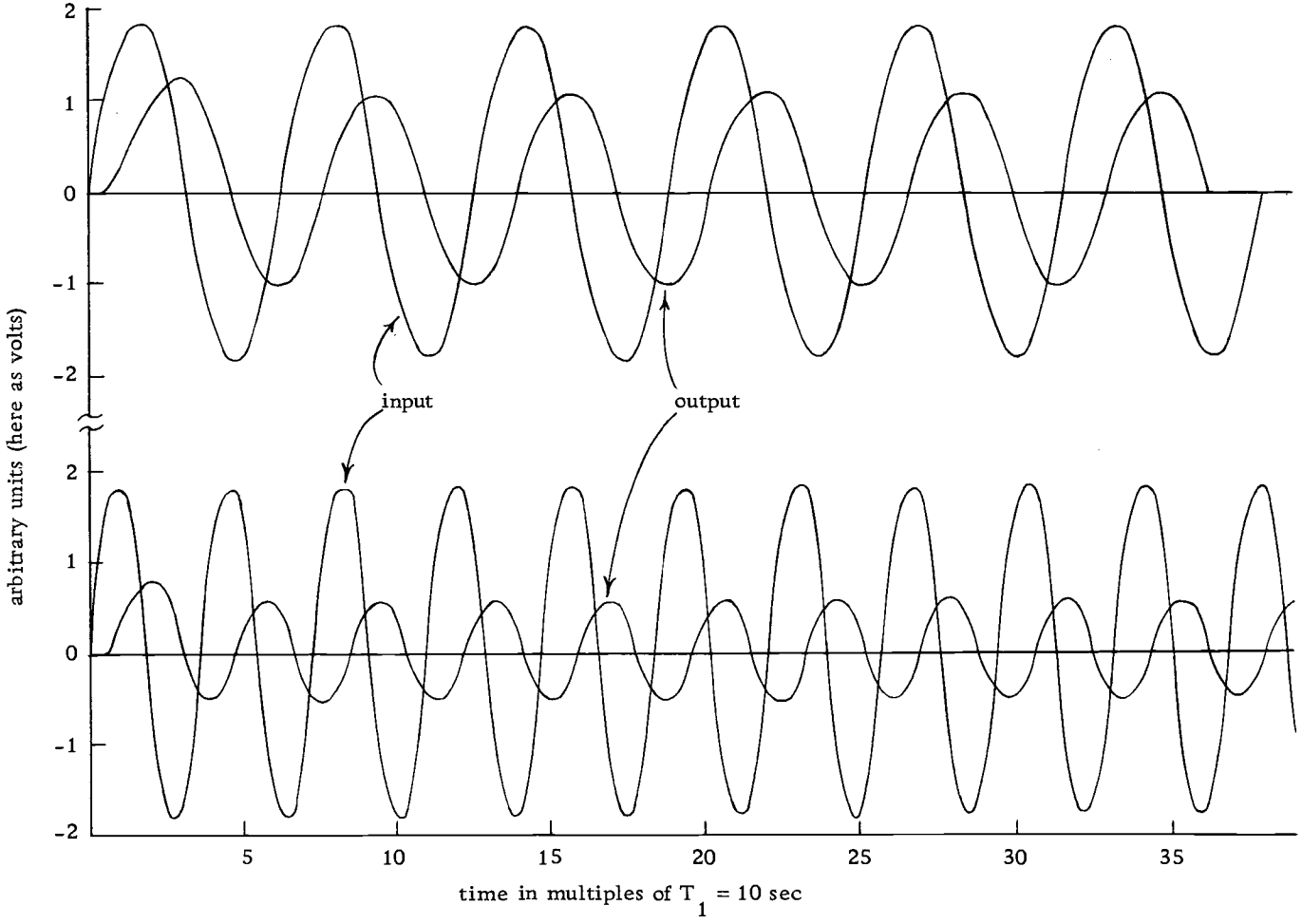

Figure 27. Simulated transition curves for sinusoidal inputs.

$$\phi = -\sum_{i=1}^{i=n} \tan^{-1} \frac{2\pi T_i}{\tau} \qquad (21)$$

Knowing the response of a system to sinusoidal inputs is important because any periodic function can be synthesized by the appropriate Fourier series summation of sinusoidal signals.

The gain and phase angle of a system are two additional "figures of merit." Bode plots for the frequency response and phase angle of the model, in which $n = 2$ and $T_2 : T_1 = 0.61$, are shown in Figures 28 and 29. In these figures the points represent actual measured values while the lines correspond to the values calculated from Equations 20 and 21 respectively. It is these characteristics which determine the stability of a feedback control system. It is possible, as is indicated by Equation 21, for a continuous analysis system to provide a 180° phase shift to a sinusoidal input. Even though the gain for such a response is small, high gains elsewhere in the feedback loop (gains of -10^4 are common) provide sufficient signal for normal negative feedback controllers to go into oscillation (an unstable condition). Clearly small phase angles are desirable.

Results and Discussion

It is clear from the investigation of the mathematical and electronic models of continuous analysis systems, that there are two parameters and one group of parameters which are of primary

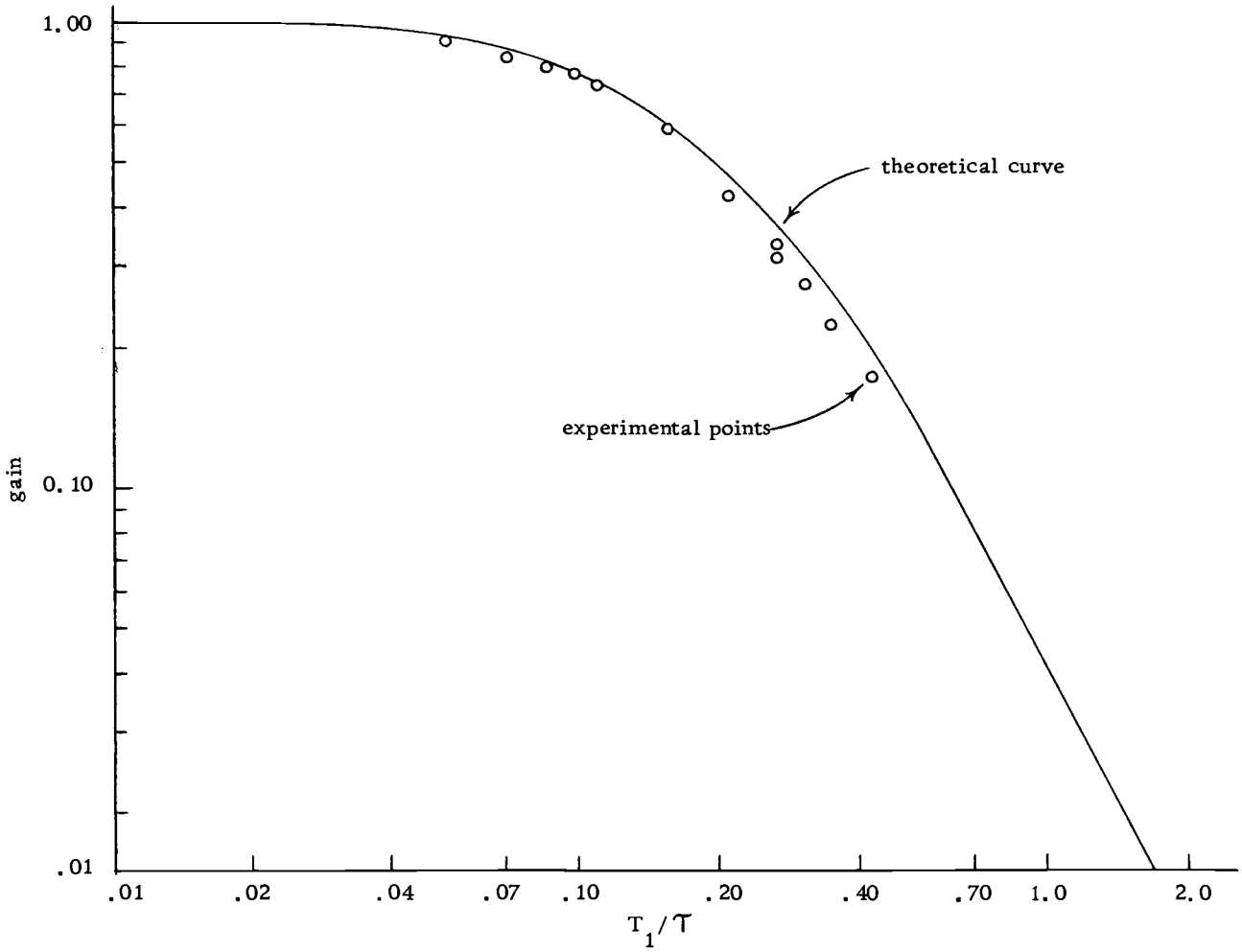

Figure 28. Bode gain plot for simulator.

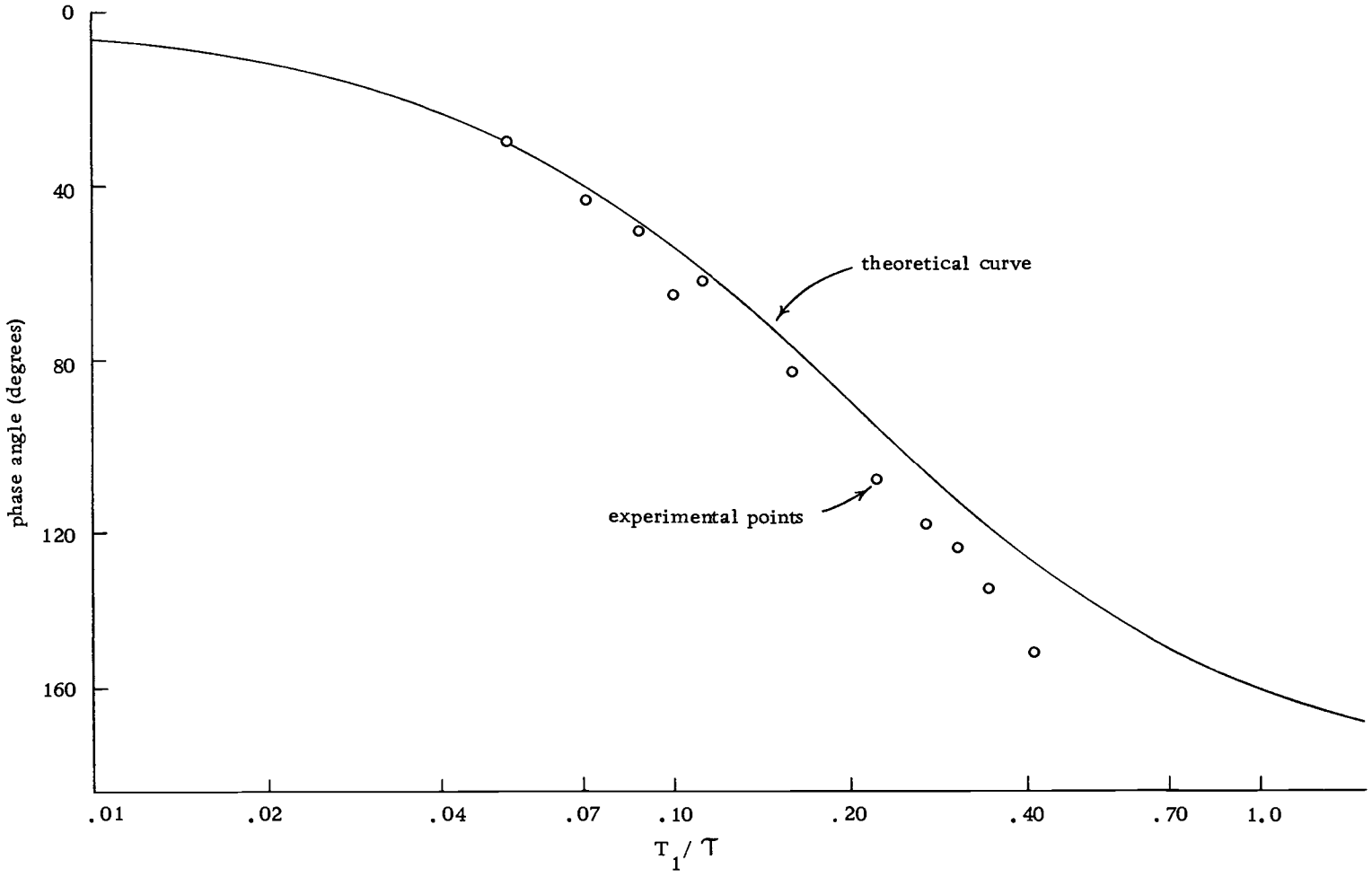

Figure 29. Bode phase angle plot for simulator.

importance to the response of such a system. These are the delay time t_d, the number of capacitive elements n, and the time constants $T_1, T_2 \ldots, T_n$ of those particular elements. Any designer setting out to optimize the apparatus used in continuous analysis, must concern himself with these parameters in accordance with the "figures of merit" discussed in the previous section.

The next step in an investigation of these important parameters, is the assignment to them of some physical significance. Fortunately there is a strong analogy between electronic and fluid systems which might provide some insight into such an investigation (25). The direct analogy between electrical potential v and fluid pressure P, between current i and flow rate Q, between the quantity of electrical charge q and volume U, is obvious. It takes only a slight extension in thought to make the comparison of electrical quantities defined in terms of potential, current, and electrical charge to their fluid analogs. Such an analogy is illustrated in Table 2. The relationship between pressure and flow rate for incompressible fluids and laminar flow is well understood (25) in terms of the Hagen-Poiseuille law. The fluid resistance can be given by:

$$R = \frac{128\mu\ell}{\pi d^4} \tag{22}$$

where μ is the fluid viscosity, ℓ and d are the length and diameter of the tube. Similarly the fluid inductance I, called inertance

because it comes from inertia forces, can be given by:

$$I = \frac{\rho \ell}{4\pi d^2} \tag{23}$$

where ρ is the density of the fluid.

Table 2. Electronic/Fluid Analogy

parameter	electronic	fluid
resistance = R	$\frac{\text{potential}}{\text{current}} = \frac{v}{i}$	$\frac{\text{pressure}}{\text{flow rate}} = \frac{P}{Q}$
capacitance = C	$\frac{\text{coulombs}}{\text{potential}} = \frac{q}{v}$	$\frac{\text{volume}}{\text{pressure}} = \frac{U}{P}$
inductance = I	$\frac{\text{potential}}{\text{rate of change in current}} = \frac{v}{di/dt}$	$\frac{\text{pressure}}{\text{rate of change in flow rate}} = \frac{P}{dQ/dt}$

Intuition would indicate that the delay time should simply be equal to the total fluid flow path volume divided by the average flow rate. In general, however, the relationship is not such a simple one. The picture is complicated somewhat by the existence of laminar flow processes which cause the solution at the center of the tube to move at twice the average velocity while the solution at the walls of the tube moves with zero velocity. Olson (20), moreover, has attributed the smearing of the sample front to a combination of laminar flow and diffusion processes.

In the electronic models $T = RC$. It seems probable (by analogy) that the various time constants in continuous analysis systems would be related to some volume divided by some flow rate. Indeed a preliminary investigation indicates that the value of T_1 for the continuous analysis apparatus of the optimization section decreases with increasing pump speed.

A comparison of the transition curves reported by Olson (20) to those reported here (Figure 22) indicates that n increases with length (or volume or wall area) of the fluid flow path. (Clearly a better understanding of the physical factors contributing to the value of n is required.) The possibility that n may be dependent on wall effects brings to attention the work of Chaney (7) who suggested that the wettability of the wall contributes to the mixing process. Table 3 compares the contact angles of a variety of construction materials (1, p. 364; 11, 12, 34). The larger the contact angle, the less wetted is the surface. Clearly almost any construction material for the fluid path would be better than glass.

Predictive Uses of the Transfer Function

If the transfer function for a continuous analysis apparatus is accurately known, it is theoretically possible, using this transfer function, to estimate the input signal by observing the instantaneous output of the apparatus. This would allow the analyst to predict the

steady state value long before that steady state is reached by the apparatus.

Table 3. Wettability of Construction Materials

Material	Contact Angle (degrees)
teflon	108
polyethylene	94
polystyrene	91
polyvinyl chloride	87
nylon	70
stainless steel	5
glass	ca. 0

In order to get the appropriate equations for this purpose, it is necessary to solve Equation 7 for V_i. If n = 2:

$$V_i = V_a[1 + (T_1 + T_2)s + T_1T_2s^2] \tag{24}$$

Expressing this equation in the time domain:

$$v_i = v_a + (T_1 + T_2)\dot{v}_a + T_1T_2\ddot{v}_a \tag{25}$$

This equation expresses the input signal v_i in terms of the instantaneous output signal v_a and its first and second derivatives.

Graphical differentiation is arduous and time consuming. A large number of points, closely spaced, are required for an accurate second derivative. A quicker and less strenuous method would be to

take the derivative electronically. While stable electronic differentiation is one of the most difficult of mathematical operations to perform, an estimated derivative can be obtained using an integrator in the feedback loop of an operational amplifier (16, p. 67). Letting the variable z be defined in terms of the function x which is to differentiated:

$$-z \equiv x + \int z\,dt - az \tag{26}$$

then:

$$x + \int z\,dt + (1 - a)z = 0 \tag{27}$$

Differentiating Equation 27:

$$\dot{x} + z + (1 - a)\dot{z} = 0 \tag{28}$$

Clearly as $a \rightarrow 1$; $-z \rightarrow \dot{x}$

Figure 30 illustrates the analog computation of Equation 26. Adjusting the potentiometer a to as close to unity as stability will allow, yields an output $-z$ as an estimated derivative of the input x.

Using circuits similar to those of Figure 30 to obtain the first and second derivative, Equation 25 was solved, for $T_1 = 10$ sec; $T_2 = 6.1$ sec., by the analog computation shown in Figure 31. Values for the potentiometer a and b of 0.910 were found to provide a usable degree of stability. The error in the estimation of the derivatives thus obtained, manifests itself largely in the second derivative. This error was offset by a 4% decrease in the computed value for the

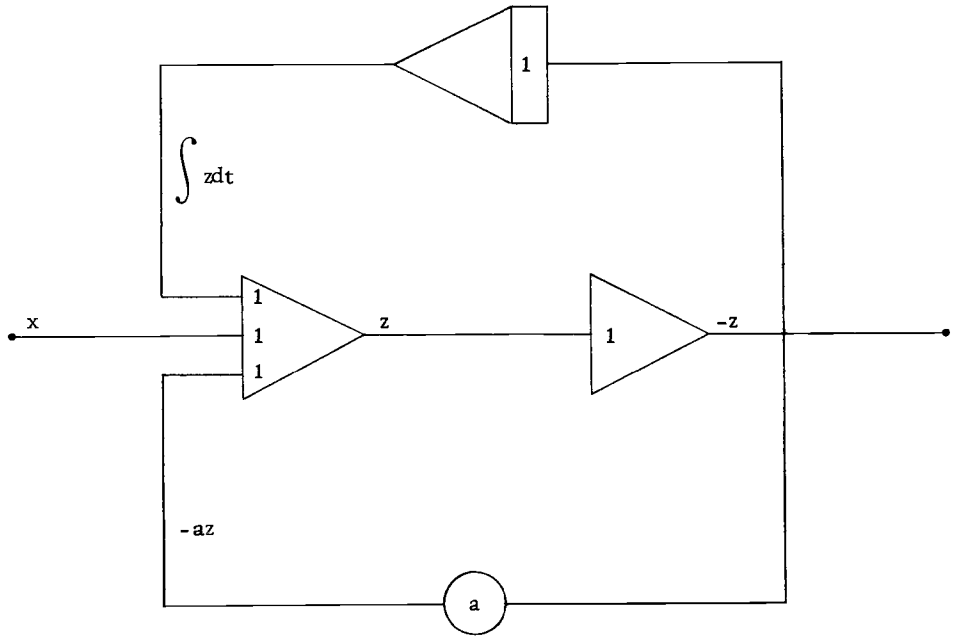

Figure 30. Approximate differentiator circuit.

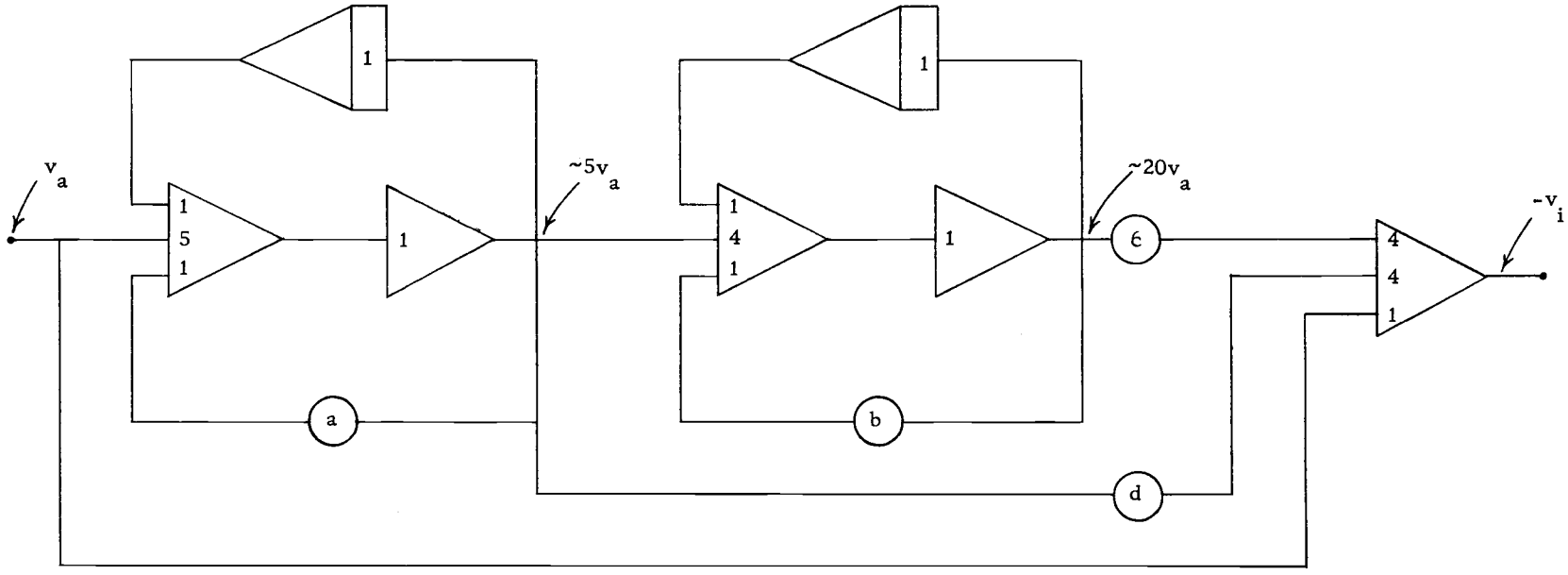

Figure 31. Second order analog computation circuit.

value of potentiometer c. The values for the scaling potentiometers then were c = 0.735 and d = 0.806.

Figure 32 illustrates the simulated continuous analyses apparatus transition curve for a step change input as compared to the equilibrium value for that transition curve computed from Equation 25 by the circuit of Figure 31. Clearly the use of predictive equations, such as Equation 25, provides an optimization to the continuous analysis process. As illustrated in Figure 32 the transition time can be reduced by a factor of twenty, leaving the transportive delay time (and associated chemical reaction times) as the major source of the response time of a continuous analysis apparatus.

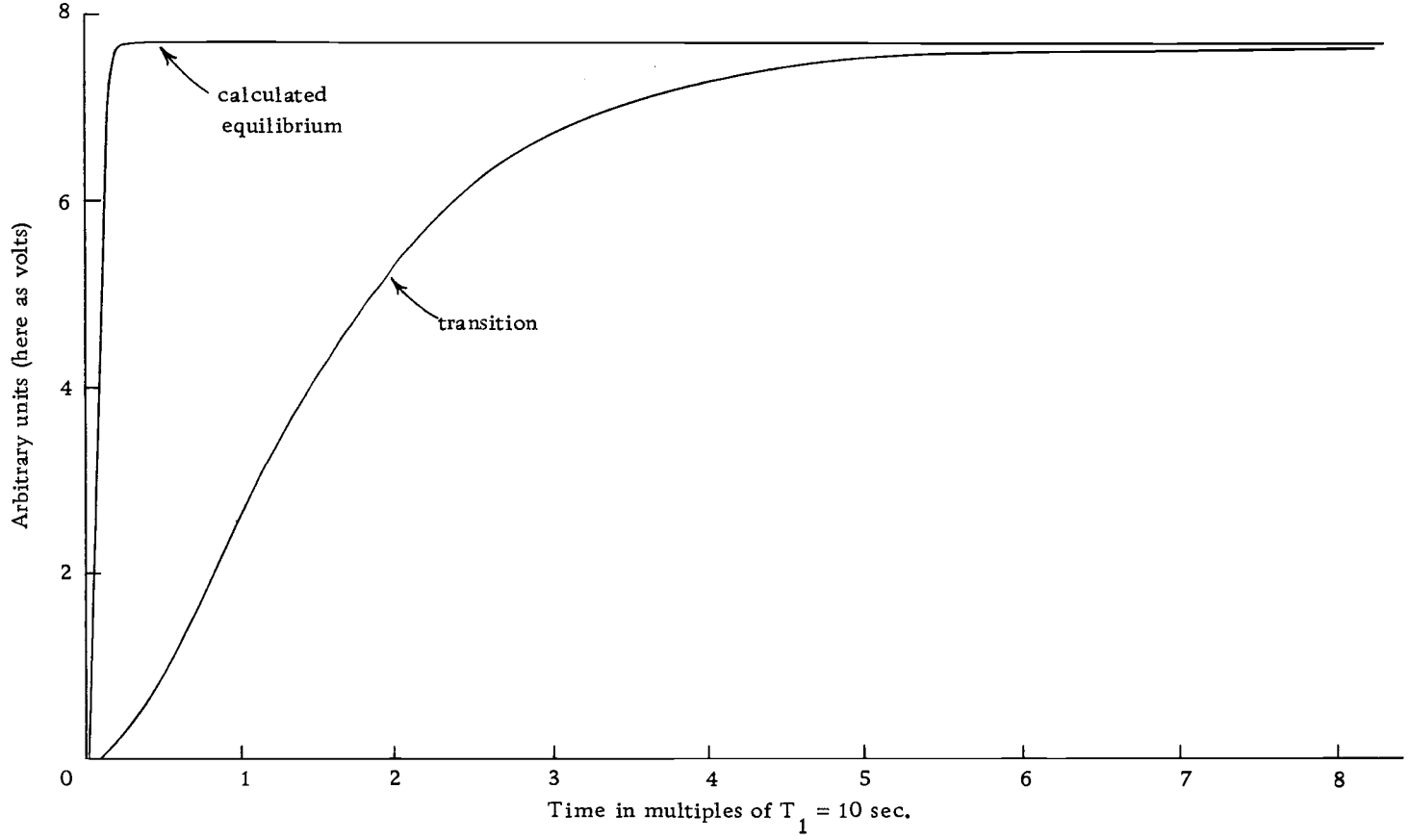

Figure 32. Simulated transition curve and calculated equilibrium value for a step input.

BIBLIOGRAPHY

1. Adamson, Arthur W. Physical chemistry of surfaces. New York, Interscience, 1967. 747 p.

2. Anderson, Arvid A. A study of the nitrosolignin test for sulphite waste liquor. B.S. thesis. Seattle, University of Washington, 1942. 45 numb. leaves.

3. Barnes, C. A. et al. A standardized Pearl-Benson or nitroso, method recommended for estimation of spent sulfite liquor or sulfite waste liquor concentration in waters. Tappi 46: 347-351. 1963.

4. Blaedel, W. J. and R. H. Laessig. Automation of the analytical process through continuous analysis. In: Advances in analytical chemistry and instrumentation, ed. by C. N. Reilley and F. W. McLafferty. Vol. 4. New York, Interscience, 1966. p. 69-168.

5. Booman, G. L. and W. B. Holbrook. Electroanalytical controlled-potential instrumentation. Analytical Chemistry 35:1793-1809. 1963.

6. Bradley, F. R. and R. McCoy. Driftless d-c camplifiers. Electronics 25:144-148. April 1952.

7. Chaney, Albert L. Applications of fluid mechanics in continuous flow systems. In: Automation in analytical chemistry, Technicon symposia 1967. Vol. I. White Plains, N. Y., Mediad, 1968. p. 115-117.

8. Clairex Corporation. Photoconductive cell design manual. New York, 1966. 15 p.

9. Crown Zellerbach Corporation. The Orzan products. Camas, Washington, n.d. 17 p.

10. Degens, Egon T., Johannes H. Reuter and Kenneth N. F. Shaw. Biochemical compounds in offshore California sediments and sea water. Geochimica et Cosmochimica Acta 28:45-66. 1964.

11. Ellison, A. H. and W. A. Zisman. Wettability of halogenated organic solid surfaces. Journal of Physical Chemistry 58: 260-265. 1954.

12. Ellison, A. H. and W. A. Zisman. Wettability studies of nylon, polyethylene terephthalate and polystyrene. Journal of Physical Chemistry 58:503-506. 1954.

13. Fellicetta, Vincent A. and Joseph L. McCarthy. Spent sulfite liquor X. The Pearl-Benson, or nitroso, method for the estimation of spent sulfite liquor concentration in waters. Tappi 46:337-347. 1963.

14. Golay, M. J. E. Height equivalent to a theoretical plate of an open tubular column lined with a porous layer. Analytical Chemistry 40:382-384. 1968.

15. Goldschmid, Otto and L. F. Maranville. Improved spent sulfite liquor determination by the nitrosolignin method. Analytical Chemistry 31:370-374. 1959.

16. Johnson, C. L. Analog computer techniques. New York, McGraw-Hill. 1956. 264 p.

17. Kester, Dana R. et al. Preparation of artificial seawater. Limnology and Oceanography 12:176-179. 1967.

18. Landee, R. W., D. C. Davis and A. P. Albrecht. Electronic designers' handbook. New York, McGraw-Hill, 1957. 1029 p.

19. Larsen, Ralph I., Ferris B. Benson and George A. Jutze. Improving the dynamic response of continuous air pollutant measurements with a computer. Journal of the Air Pollution Control Association 15:19-22. 1965.

20. Olson, Gary G. Automation of the Pearl-Benson method for spent sulfite liquor. Ph.D. thesis. Corvallis, Oregon State University, 1967. 123 numb. leaves.

21. Olson, Gary G., Roger Blaine and Harry Freund. Progress report on research on automatic and continuous methods of chemical analysis. Corvallis, Oregon State University, Department of Chemistry, 1966. 70 numb. leaves.

22. Sanderson, H. P., P. E. Penner and Morris Katz. Time constant of a Thomas Autometer and significance of indicated response. Analytical Chemistry 36:2296-2301. 1964.

23. Savant, C. J., Jr. Control system design. New York, McGraw-Hill, 1964. 457 p.

24. Shain, Irving, J. E. Harrar and G. L Booman. Simplified use of transfer functions in analysis of operational amplifier electroanalytical instrumentation. Analytical Chemistry 37:1768-1769. 1965.

25. Shearer, J. L., A. T. Murphy and H. H. Richardson. Introduction to system dynamics. Reading, Massachusetts, Addison-Wesley, 1967. p. 59-69.

26. Shilling, G. David. Process dynamics and control. New York, Holt, Rinehart, and Winston, 1963. 260 p.

27. Shinskey, F. G. Process control systems. New York, McGraw-Hill, 1967. 367 p.

28. Skeggs, Leonard T. An automatic method for colorimetric analysis. American Journal of Clinical Pathology 28:311-322. 1957.

29. Technicon Instrument Corporation. Automation in analytical chemistry, Technicon symposia 1965. New York, Mediad, 1966. p. 237-314.

30. Technicon Instrument Corporation. Automation in analytical chemistry, Technicon symposia 1966. Vol. I. White Plains, N. Y., Mediad, 1967. p. 542-583.

31. Technicon Instrument Corporation. Automation in analytical chemistry, Technicon symposia 1967. Vol. I. White Plains, N. Y. Mediad, 1968. p. 329-392.

32. Technicon Instrument Corporation. Automation in analytical chemistry, Technicon symposia 1967. Vol. II. White Plains, N. Y., Mediad, 1968. p. 355-410.

33. Thiers, R. E., R. R. Cole, and W. J. Kirsch. Kinetic parameters of continuous flow analysis. Clinical Chemistry 13: 451-467. 1967.

34. Trevoy, D. J. and Hollister Johnson, Jr. The water wettability of metal surfaces. Journal of Physical Chemistry 62:833-837. 1958.

35. Wilburn, F. W., J. R. Hesford and J. R. Flower. Use of an analog to improve the performance of a differential thermal analysis apparatus. Analytical Chemistry 40:777-788. 1968.

APPENDIX

APPENDIX

ELECTRONIC CIRCUIT CARD CONSTRUCTION

Much of the electronic circuit of the colorimeter has been built on type 837 epoxy paper "plugboards" (Vector Electronics Co., Glendale, California 91201). These 4.5 × 3-inch epoxy paper boards have a grid of 0.062-inch holes on 0.1-inch centers and are fitted with a series of 12 contacts which mate with type R 612-1 sockets (Elco Corp., Willow Grove, Penn. 19090). To each card is added a Vero type 10036 handle to aid in withdrawing the boards from restricted areas. Vector type T28 push-in terminals are used as soldering terminals. Use of these circuit cards permit easy access to a particular portion of the electronic circuit for testing or trouble-shooting purposes. Four such circuits cards are used: a power supply card (Figures 33 and 34), a lamp supply card (Figures 35 and 36), an operational amplifier circuit card (Figures 37 and 38) and a switching circuit card (Figures 39 and 40). The remaining portion of the electronic circuitry, such as controls, transformers and large capacitors, are mounted on the chassis proper (Table 6 and Figure 41).

A number of wiring practices are common to all of the cards and to the main chassis. These include assignment of card contacts to particular functions, color coding, and heat dissipation.

Each of the twelve contacts on the plugboards is assigned a particular function, or point in the total circuitry. This is designed to serve as a safety factor so that if a circuit board is inadvertently plugged into the wrong socket, no portion of the circuit will be irreparably damaged. The contact assignments are shown in Table 5.

A systematic form of color coding is used throughout the electronic circuitry. The colors red and yellow are used to denote positive and negative direct current supply voltages. Orange coloring indicates an alternating current supply. Signal and ground are denoted by the colors green and black, respectively.

Circuit components which will generate a certain amount of heat in their operation (eg. power resistors) are mounted away from the circuit board to aid ventilation. Type NF205 (Wakefield Engineering, Inc., Wakefield, Mass. 01880) heat sinks are provided for the transistor T_5 and diodes D_{10} and D_{11}. A 3/8 × 2 × 3-inch steel plate is mounted between the bodies of the TRIAC's (D_5, D_6, D_{18}, D_{19}) and the plugboard to aid in their heat dissipation. The power transistor T_6 is mounted directly on the main chassis for maximum heat sinking.

Table 4. Electronic Component List

C_1	= 1.0 mfd, 25v	R_4	= 1 meg variable
C_2	= 200 pfd	R_5, R_6	= 3.9 k
C_3	= 0.5 mfd, 400 v	R_7, R_8, R_{29}	= 1.5 k
C_4, C_5	= 120 mfd, 450 v	R_9, R_{10}	= 6.8 k
C_6	= 36,000 mfd, 15 v	R_{11}, R_{12}, R_{27}	= 470
C_7, C_9	500 mfd, 15 v	$R_{13}, R_{14}, R_{33}, R_{34}$	= 100
C_8	= 0.0047 mfd	R_{15}, R_{17}	= 10 k, 1%
C_{10}	= 1.0 mfd, 400 v	R_{16}	= 10 k ten turn precision
$D_1, D_2, D_{14}, D_{15}, D_{16}, D_{17}$	= 1N316	R_{18}	= 100 k variable
D_3, D_4	= 1N750	R_{19}, R_{20}	= 2.37 k, 1%
D_5, D_6, D_{18}, D_{19}	= 40429	R_{21}, R_{22}	= 3.0 k, 20 w
D_7, D_8	= 1000 piv. 1 a	R_{23}, R_{24}	= 10 k, 2 w
D_9	= MDA 952-1	R_{25}	= 4.7 ohm
D_{10}, D_{11}	= 1N3794A	R_{26}	= 100 k variable trimmer
D_{12}, D_{13}	= VR56A	R_{28}	= 500, 5 w
F_1	= 3/4 amp SLO BLO	R_{30}	= 10 k variable trimmer
F_2	= 1/4 amp SLO BLO	R_{31}	= 82
F_3	= 5 amp	R_{32}	= 560
L_1	= neon pilot lamp	S_1	= SPST
M	= 100-0-100 a meter	T_1, T_4	= 2N1304
M1	= fan motor	T_2, T_3, T_5	= 2N1305
MO	= 1 rpm reversible motor	T_6	= TR-02
OA	= MC 1709 CG	XFMR1	= 135 v @ 200 ma, 6.3 v @ 5.5 a.
R_1, R_3	= CL 607L photo-conductor		
R_2	= 10 k variable		

Table 5. Plugboard Contact Assignments

Pin Number	Function
1	115 vac for balancing motor
2	115 vac for balancing motor
3	115 vac auxilary
4	signal (input)
5	signal (output)
6	ground
7	-16 v or regulated lamp supply
8	-56 v or unregulated lamp supply
9	-150 v
10	+16 v
11	+56 v
12	+150 v

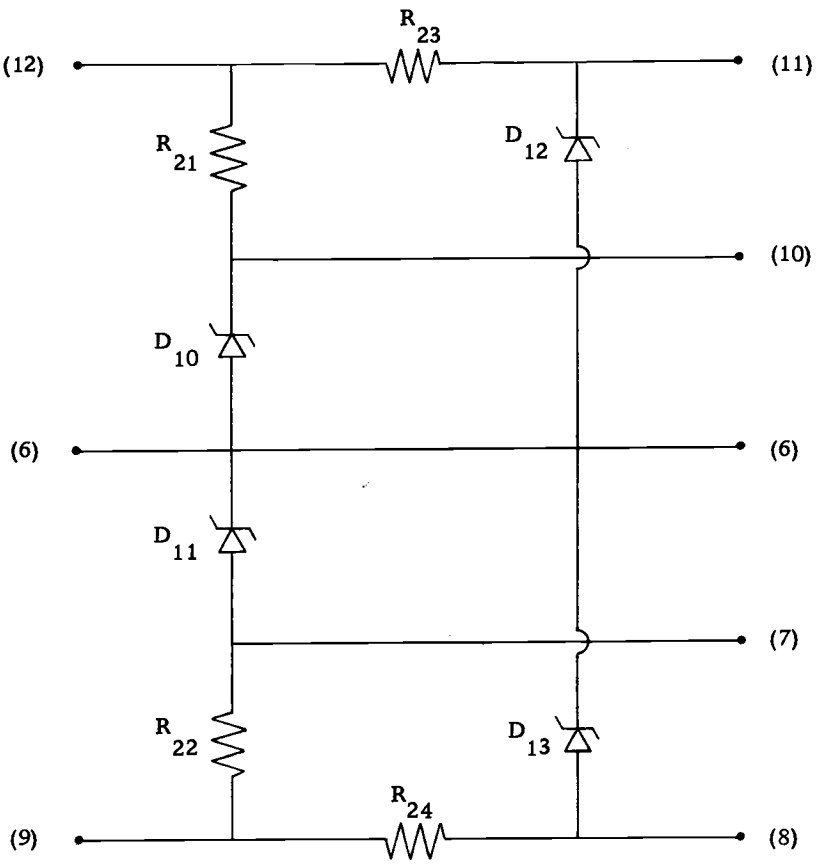

Figure 33. Power supply card circuit diagram.

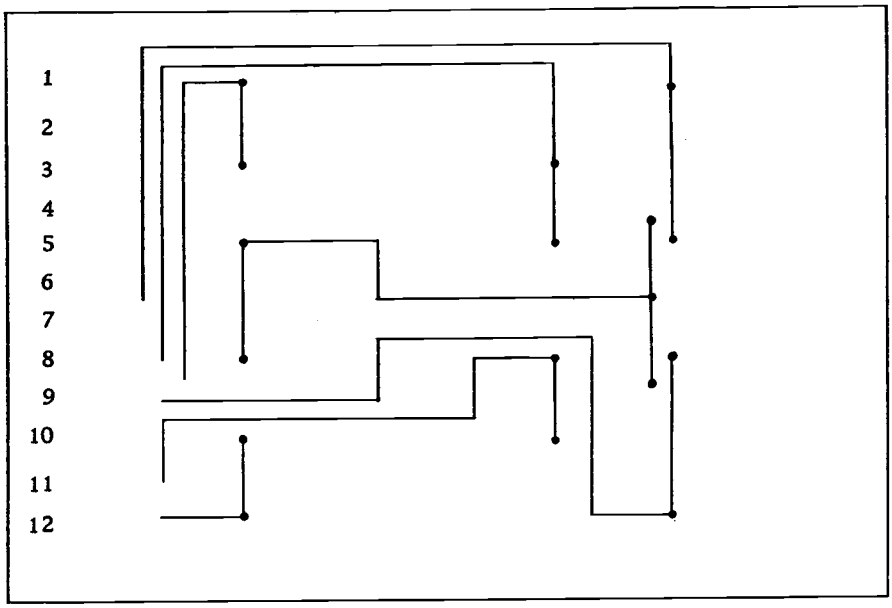

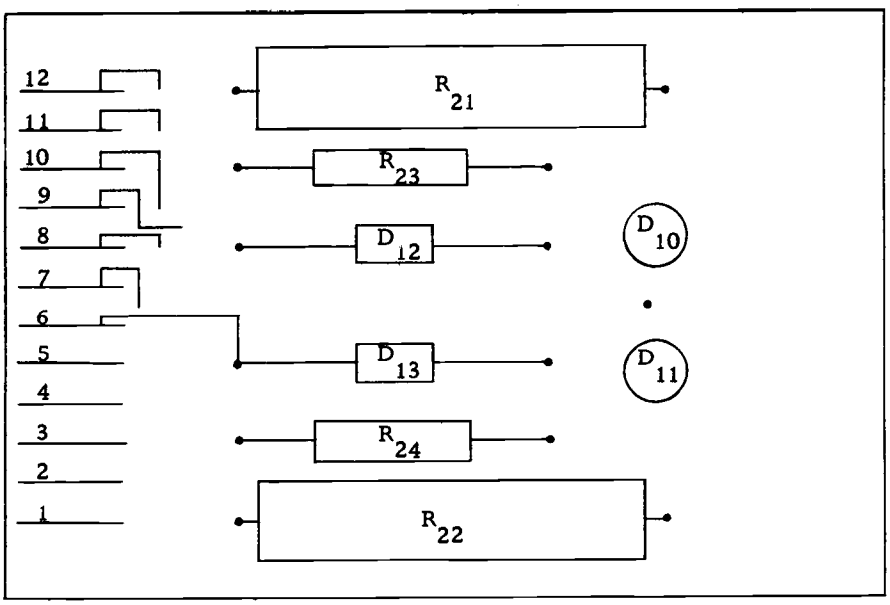

Figure 34. Power supply card layout diagram.

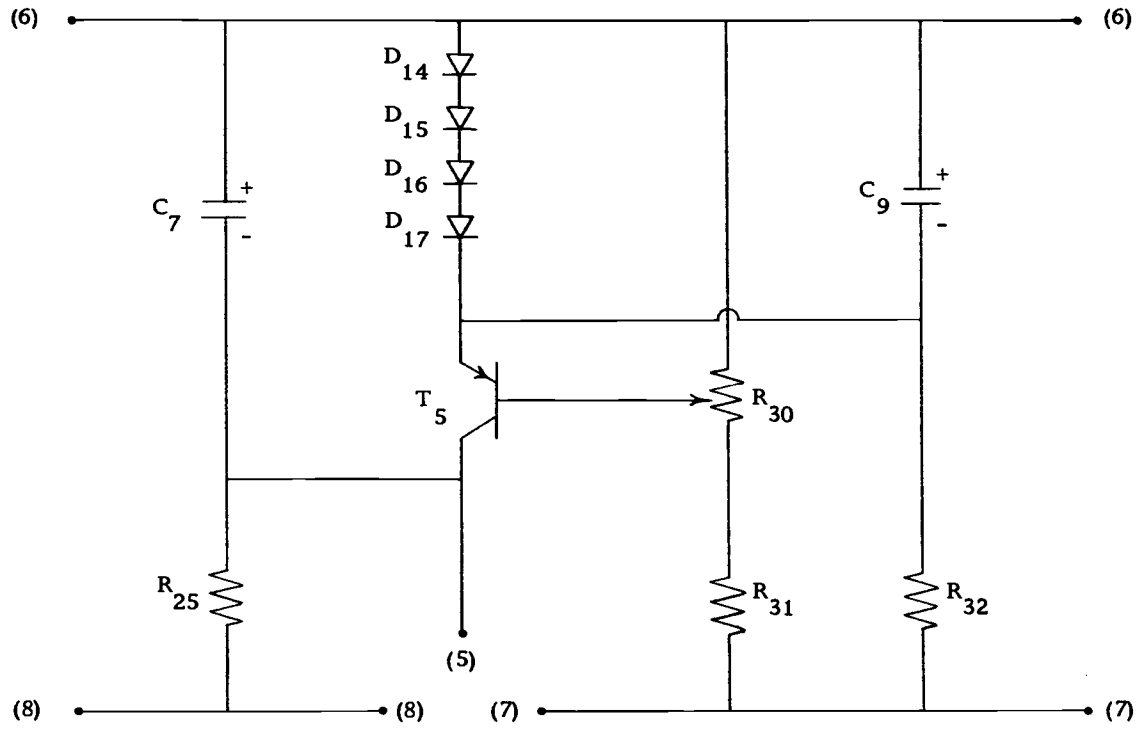

Figure 35. Lamp supply card circuit diagram.

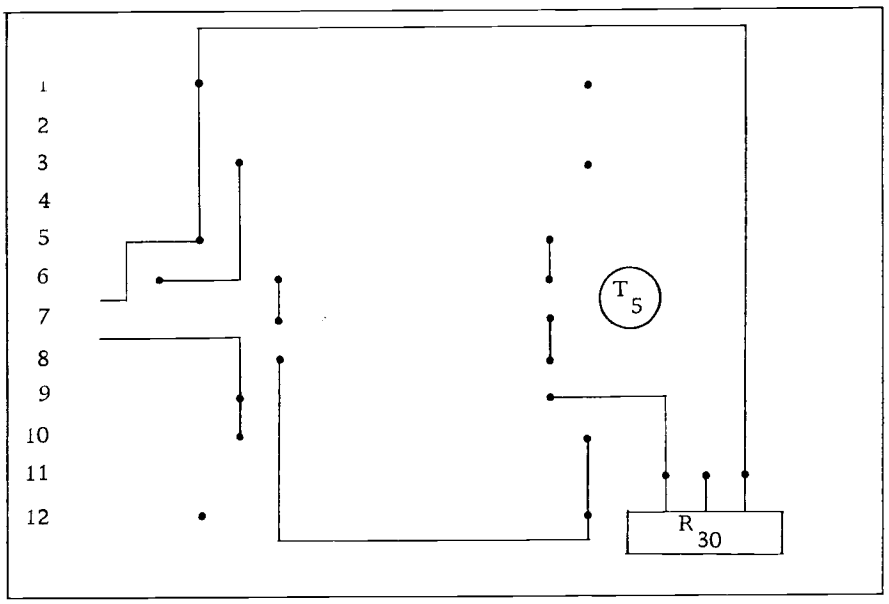

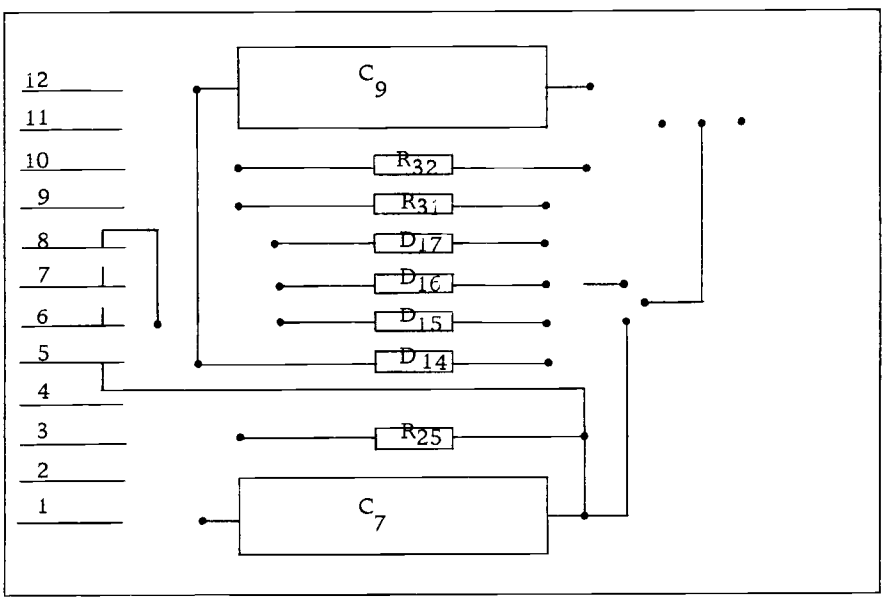

Figure 36. Lamp supply card layout diagram.

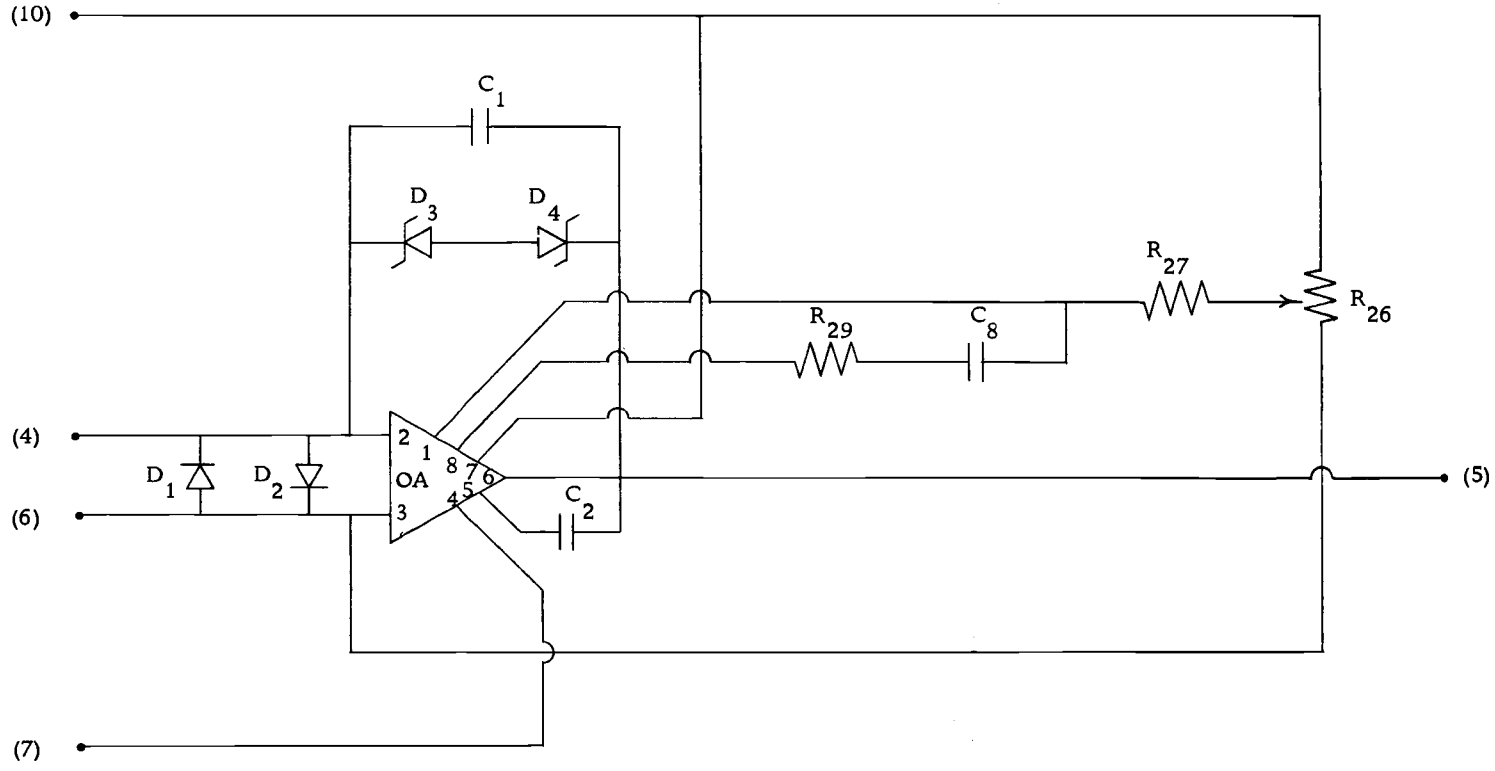

Figure 37. Operational amplifier circuit card circuit diagram.

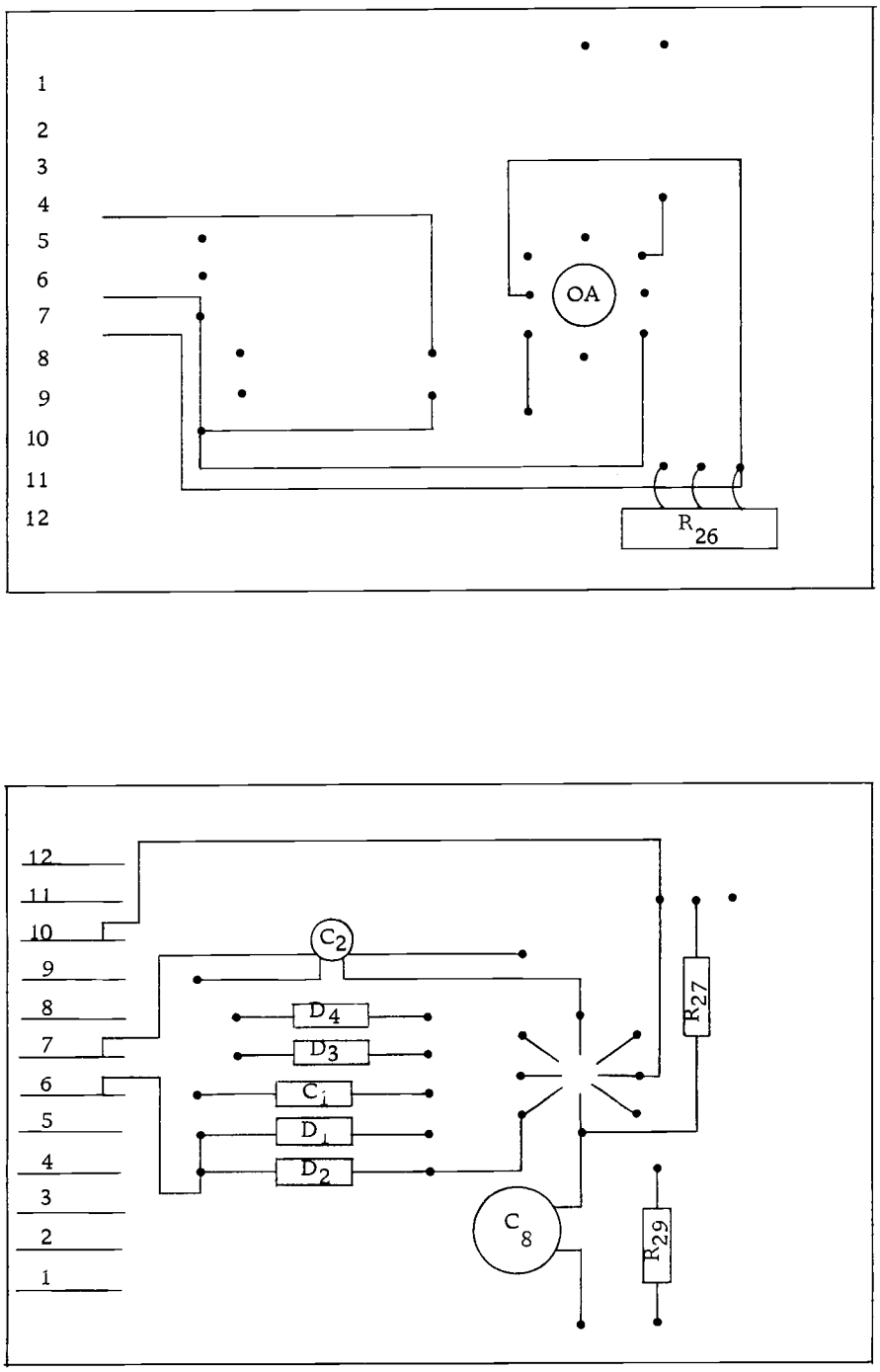

Figure 38. Operational amplifier circuit card layout diagram.

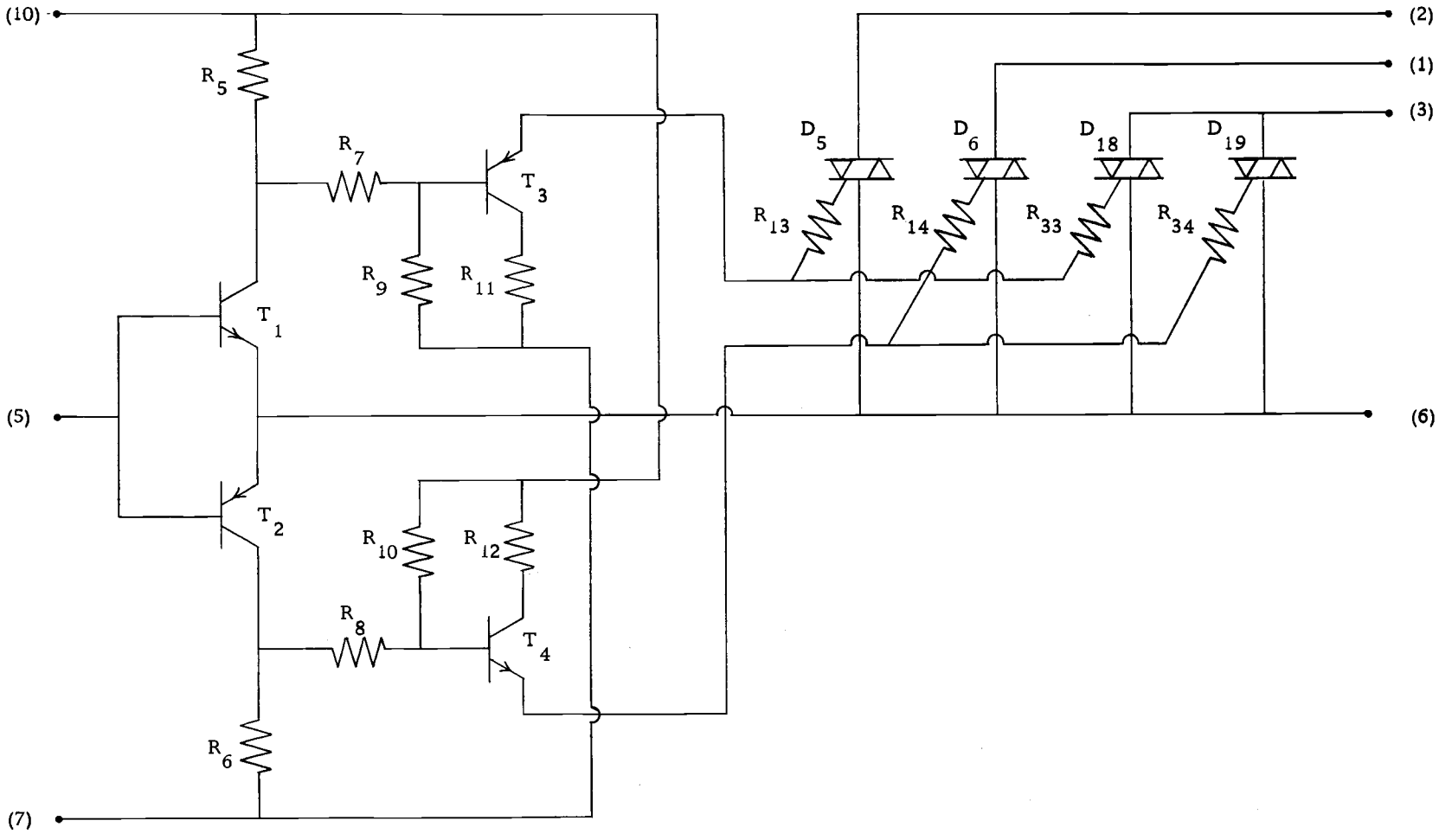

Figure 39. Switching circuit card circuit diagram.

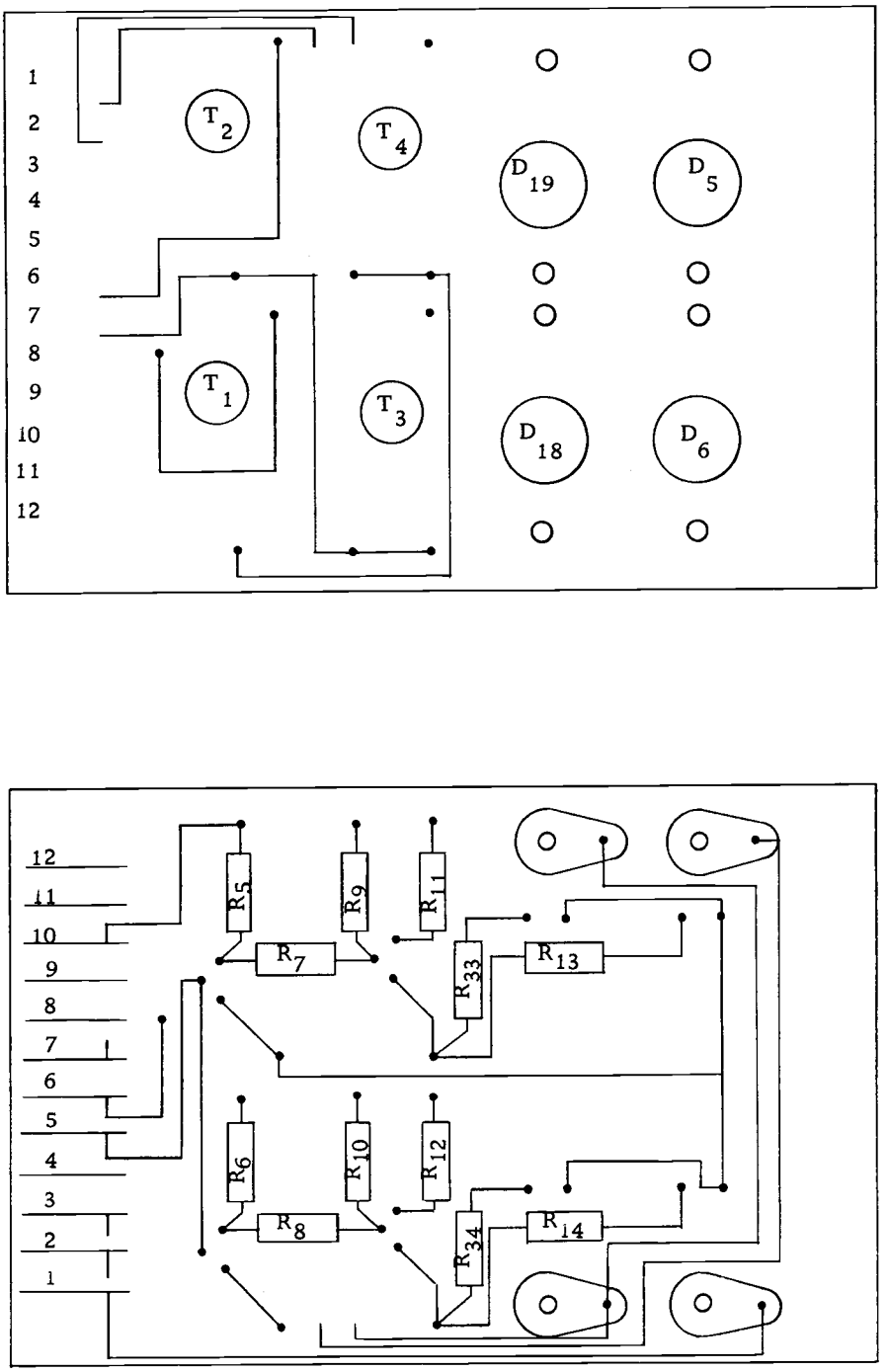

Figure 40. Switching circuit card layout diagram.

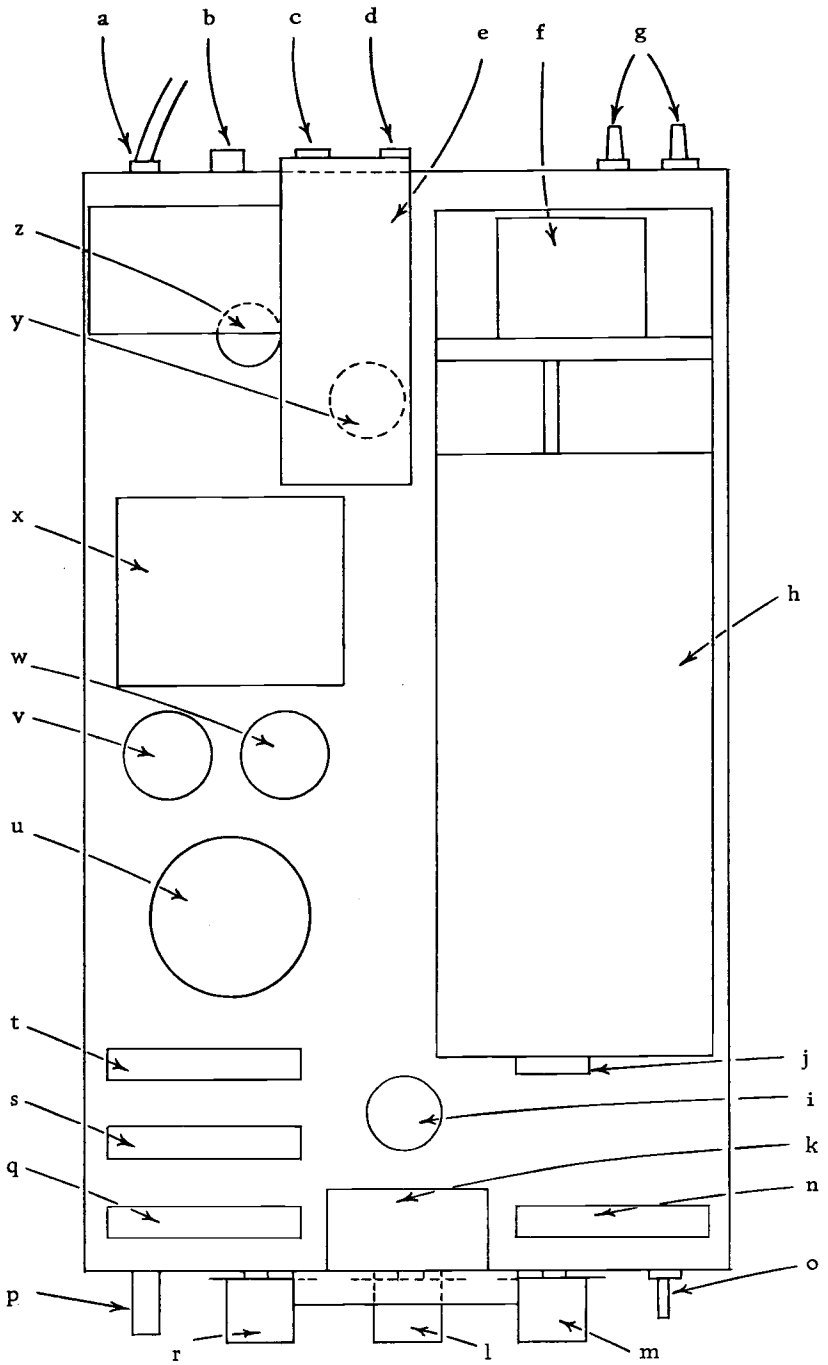

Figure 41. Colorimeter layout (scale 3:1).

Table 6. Component List for Colorimeter Layout

a	line card input
b	fuse holder for F_3
c	fuse holder for F_2
d	fuse holder for F_1
e	ventilation fan
f	balancing motor
g	fluid connectors
h	optical box
i	cable connector
j	cable connector
k	meter
l	beam balance control, R_2
m	calibration control, R_{18}
n	switching circuit card
o	power switch, S_1
p	readout terminals
q	operational amplifier card
r	sensitivity control, R_4
s	lamp supply card
t	power supply card
u	capacitor, C_6
v	capacitor, C_5
w	capacitor, C_4
x	transformer, XFMR1
y	cable connector
z	power transistor, T_6

PEARL-BENSON REACTION

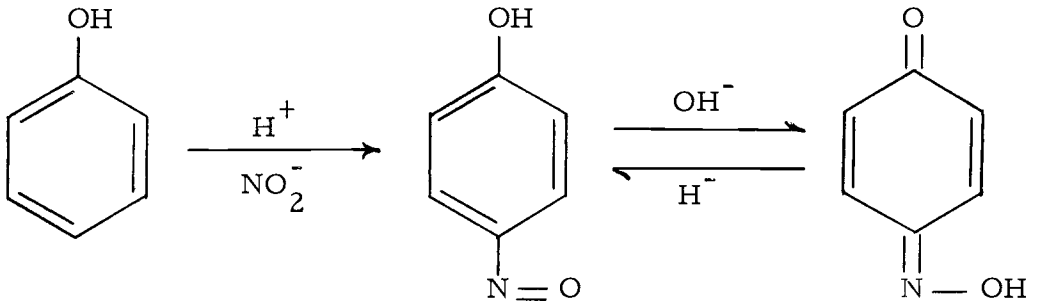

phenol nitrosophenol quinone mono oxime

Figure 42. The Pearl-Benson Reaction.

Lignosulfonates are high molecular weight compounds based on p-hydroxybenzoyl, vanillyl, and syringyl monomeric species. This phenolic polymer behaves, in the Pearl-Benson reaction, as does the phenol illustrated above.